Rev. Adv. Mater. Sci. 30 (2012) 27-59

NONLINEAR WAVE PROPAGATIONS IN SOLIDS AND THE CORRELATED DYNAMIC BEHAVIOR OF MATERIALS - AN OVERVIEW OF THE RELATED RESEARCH WORKS BY WLL GROUP IN CHINA

Lili Wang, Danian Chen, Liming Yang, Fenghua Zhou and Xinlong Dong

Mechanics and Material Science Research Center, Ningbo University, China

Received: August 08, 2011

Abstract. This article briefly overviews the research works conducted by the Wang Lili group in China, in the fields of *Explosion Mechanics* and *Impact Dynamics*.

Unlike the static cases, the mechanical responses of structures or materials under explosive/ impact loadings involve stress wave propagations and dynamic deformation-failure properties of materials. This research has significant practical values in civil and defense applications, and is a research frontier in the disciplinary areas of mechanics and material science. Over more than twenty years, the group, leaded by Professor Lili Wang and actively worked by the faculty team, has been focusing its research interests in this area. The major results obtained so far include:

- Propagating properties of loading-unloading boundary due to the elastic plastic wave velocity discontinuity across boundary. We have established a fundamental approach to study the boundary propagating behavior, and studied further the corresponding unloading failure of materials.
- The constitutive theory of nonlinear viscoelastic material and its application: A model describing the weak-nonlinear viscoelastic properties of polymers under different strain-rates is proposed and used to analyze the propagating character of viscoelastic stress waves. Applying this wave analysis, we proposed a viscoelastic Hopkinson bar system to measure the dynamic properties of soft materials.
- Dynamic failure due to stress wave propagations: For spallation induced by reflected unloading waves, a stress-release mechanism in the coalescence process of micro-damage is proposed, a crack-evolution equation based on a critical fragment volume is presented, and a new crack straining based spall model is established. For fragmentation of brittle materials, taking account of nucleation, growth and interaction of cracks, a new model is built, which promotes the studies on fragmentation under different strain-rates. For thermo-viscoplastic constitutive instability of materials under quasi-adiabatic impact, a macroscopic criterion for predicting the evolution of micro-adiabatic shear bands is proposed, the coupled relation between shear banding and crack extension is formulated, and the influence of geometrical factors on adiabatic shearing is revealed.
- Engineering application based on the combining studies on stress waves and material dynamic behavior, such as bird-strike on aircrafts, ship-bridge collision and defense engineering: Based on impact dynamics analysis, a new flexible, energy-consuming crash-proof device against ship-bridge collision is developed for first time, showing that the impact force is markedly decreased, the duration under lower impact-force is prolonged, and the ship is able to turn its navigation direction and thus the device protects both ship and bridge. This new device has been applied for the bridge across Zhanjiang bay, saving more than RMB 400 millions.

Those results will be highlighted in the following parts.

Corresponding author: Lili Wang, e-mail: wanglili@nbu.edu.cn

1. RESEARCH BACKGROUND

Unlike the cases under static loadings, the mechanical responses of structures under explosive/impact loadings involve stress wave propagations and the correlated dynamic response of materials. Such research is urgently required in civil and defense engineering, and is an international research hot-spot. Specifically, detailed research is required on the complicated phenomena such as: nonlinear elastic-plastic waves involving large deformation, nonlinear viscous waves involving rate-effects, unloading waves involving unloading properties of solids, failure due to stress wave interactions, dynamic fracture and unloading waves induced by failure, and so on. As the phenomena generally associate multi-physical mechanism an interdisciplinary research of mechanics, material science, and other sciences are needed.

For the dynamic process characterized by stress wave propagation, which involves both loading waves and unloading waves and their interaction, the difficulty lies in the determination of loading-unloading boundaries since they are unknown in advance. Because the nonlinear constitutive equations of material are different in loading and unloading process, the propagation of loading-unloading boundary becomes very complicated, and the systematical investigation is insufficient. Correspondingly, with regard to the structure strength, the researchers until recently mainly give attention to the “loading failure”, while the “unloading failure” frequently takes place under conditions of wave propagation, of which systematical investigation is also insufficient. For example, neither the “front spalling” phenomenon appearing near the loading surface due to plastic unloading waves, nor the mechanism of formation of many annular surface cracks during solid particle erosion have been studied sufficient.

The propagating characters of stress waves strongly depend on the dynamic constitutive behavior of materials. In fact, real solids all display rate-dependent viscosity in varying degrees. Therefore, rate-dependent constitutive relation and rate-dependent wave propagation should be simultaneously studied. Since most of previous research works in this area are limited to linear situation, problems of nonlinear viscoelastic constitutive relation and the corresponding wave propagation, either direct problems or inverse problems, are require to deep study both theoretically and experimentally. As to the experimental investigation of rate-dependent constitutive relation of materials, since the traditional elastic Hopkinson pressure bar technique is no longer sufficient for new soft materials with low wave impedance, new technique should be solved.

Dynamic failure of structures and materials in different modes, such as spalling, fragmentation, and adiabatic shearing, all involves complicated waves and strain-rate effects. Either the rate-dependent evolution of damage and spalling due to reflected unloading waves, or the multi-sources damage evolution and fragmentation under high strain-rate loading, or the microscopic mechanism and macroscopic criterion of adiabatic shearing under high strain-rate quasi-adiabatic loading, all are unsolved interdisciplinary frontier problems, which are urgently required to study either from the view of academic study or of engineering application.

For the economical and social developments, impact defense is also an important issue. To solve the practical problems, such as bird-strike on aircrafts, ship-bridge collision and explosion-resist protect design in defense engineering, synthetic studies on stress wave propagation and rate-dependent constitutive relation are currently required by both theoretical study and practical engineering, which are also major researches thrust for the Mechanics and Material Science Research Center (MMSRC) in Ningbo University.

2. RESEARCH IDEAS

Comparing to the problems under quasi-static loading, taking account of inertia effects and strain-rate effects are the main characters and the major difficulties in an explosion/impact dynamics problem. The inertia effect leads to the study of wave propagation in various (precise or simplified) forms, promoting the development of structural impact dynamics; while the strain-rate effect leads to the study of all kinds of rate-dependent constitutive relations and failure criteria under high strain rates, promoting the development of material impact dynamics.

The main difficulty lies in that those two effects are usually inter-coupled. In fact, on the one hand, no wave propagation can be analyzed without knowing the dynamic constitutive relation of the material; consequently the basic characteristics of wave propagation inevitably depend on the strain-rate dependence of material behavior. On the other hand, in the study of dynamic constitutive relations and failure criteria of materials at high strain rates, wave propagation effects should not be neglected.

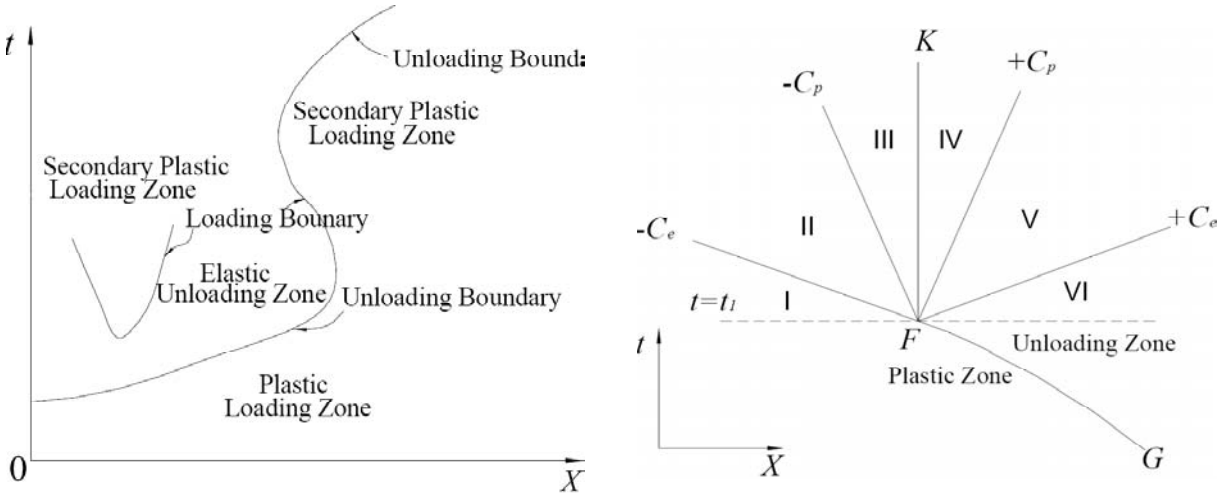

Fig. 1. (a) Two categories of elastic-plastic boundaries: loading boundary and unloading boundary; (b) Six possible zones exist for a weak-discontinuous boundary.

In fact, under a transiently applied loading (such as explosion or impact loading) with a characterized time duration T_L, structures response rapidly. In such a dynamic process, stress waves propagate within the structure due to the inertia effect. If the characterized wave velocity is C and the characterized scale of structure is L_s, then a characterized time T_W ($=L_s/C$) can be used for describing the dynamic response time of the structure. Because the wave velocity C depends on the mechanical properties of materials, the characters of stress wave propagation intrinsically depend on the dynamic behavior of the material. When $T_L<T_W$, responses of the structures cannot be analyzed precisely unless stress wave propagations are included. On the other hand, the dynamic deformation and the dynamic fracture of materials are essentially time (or rate) dependent, which can be characterized by *e.g.* an intrinsic deformation time T_D and an intrinsic fracture time T_f, respectively. T_D is determined by the dynamic viscous effect of materials such as viscoelasticity or viscoplasticity, and T_f is determined by the process of internal damage evolution or visco-fracture. Both T_D and T_f are again inter-influenced each other. Adding more difficulties, when we study the dynamic properties of a material characterized by time T_D or T_f, we have to take consideration of the stress wave propagation within both the material specimen and the experimental apparatuses. Such coupling between those two dynamic effects leads us to recognize the complexity on the one hand and the necessity on the other hand in such an interdisciplinary research cross mechanics and material science.

It should be noted that the mechanical behavior of materials under intense dynamic loading is a highly nonlinear problem. Since the structural responses are characterized by short time duration and possibly spatial localization, nonlinearities in relation to *finite deformation*, *irreversible elastic-plastic loading-unloading*, *high strain-rate dependent constitutive relation*, *dynamic damage evolution*, *dynamic fracture*, *etc* must be involved. Moreover, the four characterized times, T_L, T_W, T_D, and T_F, characterizing different physical mechanisms, are complicatedly variable. Such coupled "transient loading – inertia - stress wave - material nonlinearity - nonlinear stress wave" causes the study on *impact dynamics* to become a highly nonlinear, multi-scale and multi-physics problem. This is also the reason why the impact dynamics problem is a highly challenging research hot-point in the international world of science and engineering.

Despite all the difficulties, if we analyze the multi-mechanisms involved in the problem, it can be found that there is a principal clue in the whole problem, namely, the propagation of stress waves. In fact, stress wave on one hand is a form of dynamic loading which results in the nonlinear loading-unloading deformation and fracture, and on the other hand the nonlinear deformation/fracture will not only directly influence the propagating of stress wave but also induce complicated secondary waves. Thus, stress wave is both a conveying belt of loading and an information carrier of material nonlinearity. Stress waves and dynamic behavior of materials are closely coupled in this way, inter-influenced and inter-dependent. Therefore, peoples have to handle a hot

potato — a kind of recurrence of "whether hen before egg or egg before hen?"

In order to solve such a "hot potato" problem, some "un-coupled" treatments are usually used, such as when the mechanical behavior of material is known the propagation of complicated stress waves can be analyzed (the so-called *direct problem*); or when the propagating information of stress waves is known the impact dynamic response can be deduced (the so-called *inverse problem*). In the more complicated situation, we have to solve the coupled problem. In any situation, stress wave propagation is the main un-avoided problem to be dealt with.

Over the past 20 years, our research group focuses our research interests on the interdisciplinary studies of the stress wave propagation and the dynamic behavior of materials. Through a continuous research by combining theoretical, numerical, and experimental approaches, we completed in total dozens of scientific research projects and hundreds of civil engineering projects. A series of achievements both in scientific research and engineering application were achieved. The main achievements are categorized into four groups, namely the nonlinear stress wave propagation, the nonlinear viscoelastic constitutive model and viscoelastic wave, the rate-dependent dynamic fracture, and engineering applications. Representative results including publications are reported as follows.

3. NONLINEAR ELASTIC-PLASTIC LOADING-UNLOADING WAVES AND WAVE-INDUCED DYNAMIC RESPONSES OF STRUCTURES

3.1. Unloading waves and the propagation of loading-unloading boundaries

Under static loading, failure of structures usually takes place in a loading process. However, in a dynamic process characterized by stress wave propagation, wherein not only the propagation of loading waves and unloading waves, but also the interaction of loading waves and unloading waves should be taken into account, failure of structures may take place in an unloading process. Correspondingly, the loading zone and the unloading zone in the time-space coordinates should be distinguished. For this purpose, the key is to determine the propagation of loading-unloading boundary which is unknown in advance. Because the constitutive equation of elastic-plastic material is different for loading process and unloading process, the problem of determining the propagation of loading-unloading boundaries is very complicated even in the case of one dimensional wave propagation. Studies on this field were exploited first by T. von Karman *et al.* (1942) [1], Kh. A. Rakhmatullin (1945) [2] and E. H. Lee (1952) [3] respectively in the period of 2nd world war, and further developed by A.M. Skobeev (1962) [4], R. J. Clifton-T. C. T. Ting (1968) [5], and T.C.T. Ting (1971) [6]. Starting from the basic characters of stress wave propagation and the singularity in respect to the slope of stress-strain curve during a loading-unloading transit and vice versa, the basic rules of loading-unloading boundary propagation and the corresponding methods of how to determine the loading-unloading boundary were systematically and completely studied by the present authors in the 1980s [7-11]. The main results of our studies are as follows.

3.1.1. Loading boundary and unloading boundary

In general, the boundary between the plastic loading zone and the elastic loading/unloading zone varies with the propagation and interaction of stress waves. In the case of one-dimensional problem, the location of elastic-plastic boundary or loading-unloading boundary changes with time. In the space-time plane X-t, if the locus of this boundary is expressed by a function $X = f(t)$, then the propagating velocity of this boundary, $\overline{C}$, is:

$$\overline{C} = \frac{\mathrm{d}X}{\mathrm{d}t} = f'(t). \tag{3.1}$$

Loading-unloading boundaries can be categorized as two types. As shown in Fig. 1a, with the increase of time, if the state changes from a plastic-loading state to an elastic unloading state, then this part of boundary is called an unloading boundary, of which the propagating velocity is denoted by $\overline{C}_U$. On the contrary, if the state changes from an elastic state to a plastic-loading state, including the change from an elastic unloading state to a secondary-plastic loading state, then this part of boundary is called a loading boundary, of which the propagating velocity is denoted by $\overline{C}_L$.

Unlike a characteristic line that represents the propagating locus of a mechanical disturbance, an elastic-plastic boundary in general is not the propagating locus of a mechanical disturbance itself, but is the linking or moving locus of such critical

points *X*, wherein due to the interaction of stress waves a transition happens at time *t* either from the plastic loading state to the elastic unloading state (unloading boundary), or from the elastic (either loading or unloading) state to the plastic loading state (loading boundary). Under certain specific conditions, an elastic-plastic boundary may coincide with a propagating locus of mechanical disturbance (namely a characteristic line). Except those specific cases, in general it is necessary to distinguish the boundary propagating velocity $\bar{C}$ from the elastic wave velocity C_e and the plastic wave velocity C_p. With regard to the loading boundary, consider an arbitrary material particle on the boundary. Before the boundary passes, the particle is in an elastic loading state. After the boundary passes, the particle point is in a plastic loading state. Therefore, at the time when the boundary passes the particle, the slopes of the stress-time (σ-t) curves on the both side of the boundary have the same sign, as $(\partial\sigma^e/\partial t)/(\partial\sigma^p/\partial t) \geq 0$. Here and after the superscripts (or subscripts) "e" and "p" stand for the elastic and the plastic, respectively. However, in case that $\partial\sigma^e/\partial t = \partial\sigma^p/\partial t = 0$, we should consider the signs of the 2nd order derivatives. Before and after the loading boundary passes the particle, the curvatures of the stress-time curves changes from non-positive to non-negative (tensile loading), or changes from non negative to non positive (compressive loading). With regard to the unloading boundary, when the boundary passes the particle, the state changes from a plastic loading process to an elastic unloading process, so we have $(\partial\sigma^e/\partial t)/(\partial\sigma^p/\partial t) \leq 0$. In case that $\partial\sigma^e/\partial t = \partial\sigma^p/\partial t = 0$, before and after the unloading boundary passes the particle, the curvatures of the stress-time curves have the same signs. Summarizing the above discussions, on a loading boundary we have

$$\frac{\partial\sigma^e}{\partial t}\Big/\frac{\partial\sigma^p}{\partial t} \geq 0 \quad \text{or} \quad \frac{\partial^2\sigma^e}{\partial t^2}\Big/\frac{\partial^2\sigma^p}{\partial t^2} \leq 0, \tag{3.2}$$

while on an unloading boundary we have:

$$\frac{\partial\sigma^e}{\partial t}\Big/\frac{\partial\sigma^p}{\partial t} \leq 0 \quad \text{or} \quad \frac{\partial^2\sigma^e}{\partial t^2}\Big/\frac{\partial^2\sigma^p}{\partial t^2} \geq 0. \tag{3.3}$$

3.1.2. Elastic-plastic (loading-unloading) boundary as a singular interface

When an elastic-plastic boundary passes through a material particle, the particle either is loaded from an elastic state into a plastic state, or is unloaded from a plastic state into an elastic state. In both cases, the mechanical properties of material display an essential change. Correspondingly, as we usually assume, a discontinuity of the slope of stress-strain curve occurs. Consequently, a discontinuity of the wave velocity *C* occurs, namely we have

$$[C] = C_e - C_p \neq 0. \tag{3.4}$$

This is the present authors who first pointed out that because of the mentioned singularity in respect to the slope of the material constitutive relationship, the state variables such as stress σ and particle velocity *v* or their derivatives are discontinuous across the elastic-plastic boundary, which is actually a kind of singular interface. This singular interface is different from the wave front. A wave front represents the propagation of a mechanical disturbance in media. It is the interface between disturbed media and undisturbed media, reflecting the singularities of mechanical variables. On the other hand, when an elastic-plastic (loading-unloading) boundary propagates in media, it carries the singularities of the material constitutive property, as well as the singularities of state variables; moreover, the singularities of the material constitutive property are invariable, while the singularities of state variables may vary (e.g. changing from a strong discontinuity to a weak-discontinuity, and vice versa). Thus, we call the wave velocity discontinuity across an elastic-plastic boundary the basic singularity; accordingly, the hypothesis that the basic singularity exists is called the basic assumption.

3.1.3. Strong-discontinuous elastic-plastic boundary

The displacement continuity condition and the momentum conservation condition across a strong discontinuous elastic-plastic boundary are, respectively

$$[v] = -\bar{C}[\varepsilon], \tag{3.5}$$

$$[\sigma] = -\rho_0\bar{C}[v]. \tag{3.6}$$

Thus the propagating velocity of a strong discontinuous elastic-plastic boundary is:

$$\bar{C} = \sqrt{\frac{1}{\rho_0}\frac{[\sigma]}{[\varepsilon]}}. \tag{3.7}$$

It does not contradict Eq. (3.4) for basic singularity, so a strong-discontinuous boundary can exist.

3.1.4. First order weak-discontinuous boundary

In the case that the elastic-plastic boundary is a weak-discontinuity, the stress σ and the particle velocity v themselves are all continuous across the boundary but their derivatives are discontinuous, we have

$$\left[K_1 + \gamma_1 J_1\right] = 0, \quad \left[\frac{1}{C}\left(J_1 + \gamma K_1\right)\right] = 0, \tag{3.8}$$

where

$$K_1 \equiv \frac{\partial \sigma}{\partial t} = \rho_0 C_0 \frac{\partial v}{\partial X}, \; J_1 \equiv \rho_0 C \frac{\partial \sigma}{\partial t} = C \frac{\partial \sigma}{\partial X}, \; \gamma = \frac{\overline{C}}{C},$$

(e, p) and ρ_0 is the density of material. The two equations in Eq. (3.8) are the basic equations that a weak-discontinuous elastic plastic boundary must satisfy. Eliminating the quantity J_1 we get

$$\left[\left(1-\gamma^2\right)K_1\right] = 0, \tag{3.9}$$

By analyzing the above equation, we get an important Theorem of the elastic-plastic boundary:

Theorem 1: Unless on the whole elastic-plastic boundary $\partial\sigma^e/\partial t = \partial\sigma^p/\partial t = 0$, all the first order partial derivatives of σ and v are discontinuous, i.e. the elastic-plastic boundary is a first order weak-discontinuity of σ and v.

Therefore, the first order weak-discontinuous boundary can be determined. In fact, for unloading boundary, since $(\partial\sigma^e/\partial t)/(\partial\sigma^p/\partial t) \le 0$ (Eq. 3.3), from Eq. (3.9) $\overline{C}$ must satisfy the following inequality

$$C_e \ge \left|\overline{C}_v\right| \ge C_p, \tag{3.10}$$

which means that the successive boundary segment FP must fall into the zone II in Fig. 1b, or if GF moves from the left lower direction toward the point F, then FP must fall into the zone V, the mirror symmetry of the zone II.

With regard to the loading boundary, including the secondary plastic loading boundary, since $(\partial\sigma^e/\partial t)/(\partial\sigma^p/\partial t) \ge 0$ (Eq. 3.2), from Eq. (3.9), $\overline{C}$ must satisfy either of the following inequality:

$$C_p \ge \left|\overline{C}_L\right| > 0, \quad \left|\overline{C}_L\right| \ge C_e, \tag{3.11}$$

which means that the successive boundary segment FP must fall into either the zone IV, or the zone VI, corresponds to the first inequality or the second inequality of (3.11), respectively. In case that GF moves from the left lower direction toward the point F, then FP must fall into the zone III or the zone I. What actually happened will be determined by the specific situation has solved before the time t_1. Whatever the zone the successive boundary segment FP falls into, all situations can be solved.

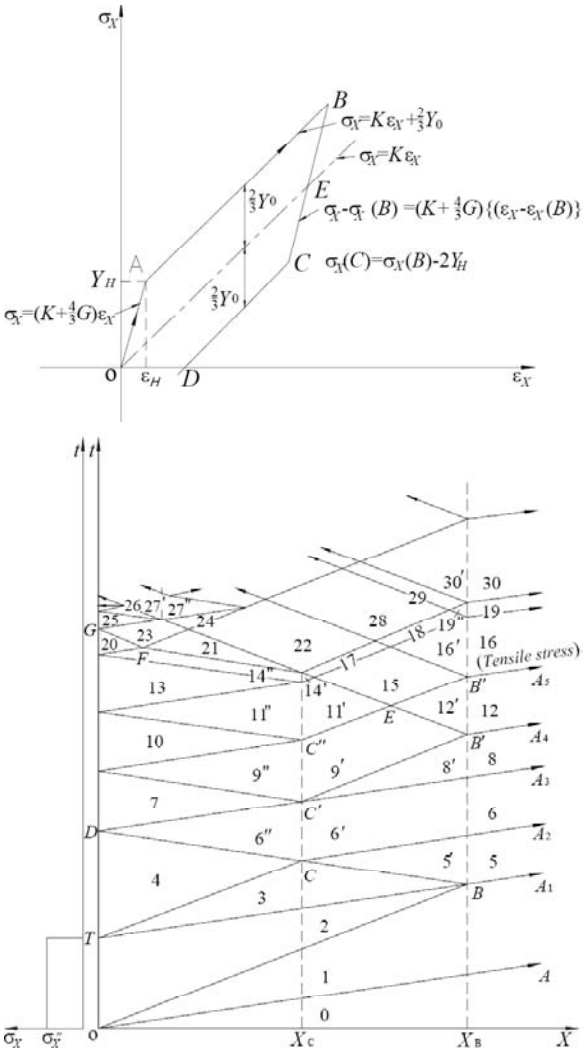

Fig. 2. (a) Axial elastic perfectly-plastic σ_X-ε_X curve in 1-D strain condition; (b) The influence of reverse plastic yield on the propagation of 1-D strain wave, resulting in the "front spalling".

3.1.5. Second order weak-discontinuous boundary

From the previous discussions about the first order weak-discontinuous boundary, we know that if across the boundary $\partial\sigma^e/\partial t = \partial\sigma^p/\partial t = 0$, then we have

$$\left[\frac{\partial \sigma}{\partial t}\right] = \left[\frac{\partial \sigma}{\partial X}\right] = \left[\frac{\partial v}{\partial t}\right] = \left[\frac{\partial v}{\partial X}\right] = 0. \tag{3.12}$$

Note that the combination of the continuation equation and the constitutive relation is satisfied on both the elastic side and the plastic side across the boundary, therefore we have $\partial v^e/\partial X = \partial v^p/\partial X =$

0. This results in another important Theorem of the elastic-plastic boundary:

Theorem 2: If across the whole elastic-plastic boundary $\partial\sigma^e/\partial t = \partial\sigma^p/\partial t = 0$, then all the first order partial derivatives of σ and v are continuous everywhere along the boundary, and both $\partial v^e/\partial X$ and $\partial v^p/\partial X$ must simultaneously be zero.

When the boundary propagating velocity becomes an indefinite form of $0/0$, it is necessary to consider the higher order derivatives of σ and v. Taking the boundary derivatives of the 1st order derivatives of σ and v, utilizing Theorem 2, we obtain

$$\left.\begin{aligned}
&\frac{\mathrm{d}}{\mathrm{d}t}\left(\frac{\partial\sigma}{\partial t}\right)=\frac{\partial^2\sigma}{\partial t^2}+\bar{C}\frac{\partial^2\sigma}{\partial t\partial X}=0,\ (e,p),\ \left[\frac{\mathrm{d}}{\mathrm{d}t}\left(\frac{\partial\sigma}{\partial X}\right)\right]=\left[\frac{\partial^2\sigma}{\partial t\partial\sigma}\right]+\bar{C}\left[\frac{\partial^2\sigma}{\partial X^2}\right]=0,\\
&\frac{\mathrm{d}}{\mathrm{d}t}\left(\frac{\partial v}{\partial t}\right)=\frac{\partial^2 v}{\partial t\partial X}+\bar{C}\frac{\partial^2 v}{\partial X^2}=0,\ (e,p),\ \left[\frac{\mathrm{d}}{\mathrm{d}t}\left(\frac{\partial v}{\partial t}\right)\right]=\left[\frac{\partial^2 v}{\partial t^2}\right]+\bar{C}\left[\frac{\partial^2 v}{\partial t\partial X}\right]=0,
\end{aligned}\right\}, \tag{3.13}$$

where the (e, p) means that the equations are suitable to both the elastic zone and the plastic zone across the boundary. Introducing

$$K_2\equiv\frac{\partial^2\sigma}{\partial t^2}=\rho_0C^2\frac{\partial^2 v}{\partial X^2}=C^2\frac{\partial\sigma^2}{\partial X^2},\ J_2\equiv\rho_0C\frac{\partial^2 v}{\partial t^2}=C\frac{\partial^2\sigma}{\partial X^2}=\rho C^2\frac{\partial v^2}{\partial X^2}. \tag{3.14}$$

Substituting them into Eq. (3.13), we can finally get

$$\left[(1-\gamma)K\right]=0. \tag{3.15}$$

By analyzing the above equation, we get another important Theorem of the elastic-plastic boundary:

Table 1. Basic relationships for determining propagation speeds of elastic-plastic boundaries.

Successive Boundary	1st order weak-discontinuous point	` The Point 2nd order weak-discontinuous point	*n*th order weak-discontinuous point
1st order weak-discontinuous boundary	$\left[K_1+\gamma J_1\right]=0$	$\left[\left(1+\gamma^2\right)K_2+2\gamma J_2\right]=0$	$\left[\phi_nK_n+\psi_nJ_n\right]=0$
	$\left[\frac{1}{C}\left(J_1+\gamma K_1\right)\right]=0$	$\left[\frac{1}{C}\left\{\left(1+\gamma^2\right)J_2+\gamma K_2\right\}\right]=0$	$\left[\frac{1}{C}\left(\phi_nJ_n+\psi_nK_n\right)\right]=0$
	$\left[\left(1-\gamma^2\right)K_1\right]=0$	$\left[\left(1+\gamma^2\right)J_2+\gamma K_2\right]=0$	$\left[\left(1-\gamma^2\right)\left(\phi_{n-1}K_n+\psi_{n-1}J_n\right)\right]=0$
	Karman *et al.* (1942)	Ting (1971)	
2nd order weak-discontinuous boundary		$K_2+\gamma J_2=0$	$\phi_{n-1}K_n+\psi_{n-1}J_n=0$
		$\left[\frac{1}{C}\left(J_2+\gamma K_2\right)\right]=0$	$\left[\frac{1}{C}\left(\phi_{n-1}J_n+\psi_{n-1}K_n\right)\right]=0$
		$\left[\left(1+\gamma^2\right)K_2\right]=0$	$\left[\left(1-\gamma^2\right)\left(\phi_{n-2}K_n+\psi_{n-2}J_n\right)\right]=0$
		Clifton and Ting (1968)	
Supplementary conditions on loading boundary	$\frac{\mathrm{d}\sigma_m}{\mathrm{d}X}=\frac{1}{\bar{C}}\left(K_1+\gamma J_1\right)$	$\frac{\mathrm{d}^2\sigma_m}{\mathrm{d}X^2}=\frac{1}{\bar{C}}\times\left\{\left(1+\gamma^2\right)K_2+2\gamma J_2\right\}$	$\frac{\mathrm{d}^n\sigma_m}{\mathrm{d}X^n}=\frac{1}{\bar{C}^n}\left(\phi_nK_n+\psi_nJ_n\right)$

Theorem 3: If across the whole elastic-plastic boundary $\partial\sigma^e/\partial t = \partial\sigma^p/\partial t = 0$, then unless on the boundary $\partial^2\sigma^e/\partial t^2$ and $\partial^2\sigma^p/\partial t^2$ are continuous, all the second order partial derivatives of s and *v* are discontinuous. In this case the elastic-plastic boundary is a second order weak-discontinuity of s and *v*.

From Eq. (3.15), the propagating velocity $\overline{C}$ of the second order weak-discontinuity can be determined by

$$\overline{C} = \sqrt{\left[\frac{\partial^2\sigma}{\partial t^2}\right] \Big/ \left[\frac{1}{C^2}\frac{\partial^2\sigma}{\partial t^2}\right]}. \qquad (3.16)$$

It is thus clear that the possible scopes of an unloading boundary velocity $\overline{C}_U$, or a loading boundary velocity $\overline{C}_L$, in the case of a second order weak-discontinuous boundary are just the counterchange of that in the case of first order weak-discontinuous boundary. The combination of those for these two cases just cover the whole possible range on the *X-t* plot from $X = -\infty$ to $X = \infty$, as shown in Fig. 1b.

Furthermore, we made further systematical analyses on the higher-than-second order weak-discontinuous boundaries, the higher order isolated points on elastic-plastic boundary, and the supplementary yield conditions on loading boundary induced by the multi-values of stress wave propagating velocity at yield stress. The corresponding basic relationships are summarized in Table 1, and more details are given in [7-11].

3.2. Dynamic failure of structures related to unloading wave propagation

Another important subject of our research is the structure failure under intense dynamic loading. Stress wave is the main form of dynamic loading which results in dynamic failure of structures. Note that an impulsive loading is in practice composed of a loading front and an unloading tail so that the incident waves are actually composed of not only a series of precursor loading waves but also a series of successor unloading waves. Although compressive stress waves are first produced by an impulsive loading, tensile stress waves will appear when compressive waves are reflected as unloading waves and interacted with the incident unloading waves or other reflected unloading waves propagating in reverse direction. Once such tensile stress caused is large enough (if a critical stress criterion is assumed) dynamic failure occurs, since for most materials their tensile strengths are much lower that their compressive strengths. Thus dynamic failure of structures under stress wave loading frequently displays in the form of unloading failure [12]. Even for the impact bending deformation of beams, the final failure mode is closely related to unloading waves [13]. The main created results of our research in this aspect are as follows.

3.2.1. The "front spalling" caused by plastic unloading waves

The "spalling" caused by unloading waves is one of most important dynamic failure phenomena for materials and structures. The so-called "back spalling", which occurs near the stress-free back surface of a plate, is the theoretical basis and key for civil blast engineering and military technology used for both offence and defense, and has been studied by predecessors. We find that, caused by plastic unloading waves, the "front spalling" may occur near the front surface where impact loading is applied [14].

As an example, consider the problem of one-dimensional (1-D) strain elastic-plastic waves propagating in an elastic-perfectly plastic body subjected to a rectangular impulse (with a loading duration of *T*) on its surface. The axial elastic perfectly-plastic σ_X-ε_X curve in 1-D strain condition is shown in Fig. 2a, wherein Y_H (=$(1-\nu)Y_0/(1-2\nu)$) is the so-called Hugoniot elastic limit, Y_0 the yield stress at 1-D stress, ν the Poisson ratio, *K* the elastic bulk modulus and *G* the elastic shear modulus [11]. Special attention will be focused on the unloading path *BECD* composing of an elastic unloading path *BC* and a plastic unloading (or reverse plastic loading) path *CD*, which is phenomenally similar to the so-called Bauschinger effect in the 1-D stress condition. Correspondingly, as shown in the *X-t* plot in Fig. 2b, at time *t*=0 an precursor elastic loading wave *OA* and a plastic loading wave *OB* will be excited simultaneously, propagating with the 1-D strain elastic wave velocity C_E ($=\sqrt{(K+4G/3)/\rho}$) and the 1-*D* strain perfectly-plastic wave velocity C_P ($=\sqrt{k/\rho} < C_E$) respectively, where ρ is the initial density of material; while at the time $t = T$ an elastic unloading wave *TB* and a plastic unloading wave *TC* will be excited simultaneously. When the faster follow-up incident elastic unloading wave *TB* catches up with and interacts with the slower incident plastic loading wave *OB* at the position X_B near the front surface, the rightward incident plastic loading wave is weakened due to the unloading effect from *TB*, while an internal reflected wave *BC* propagates

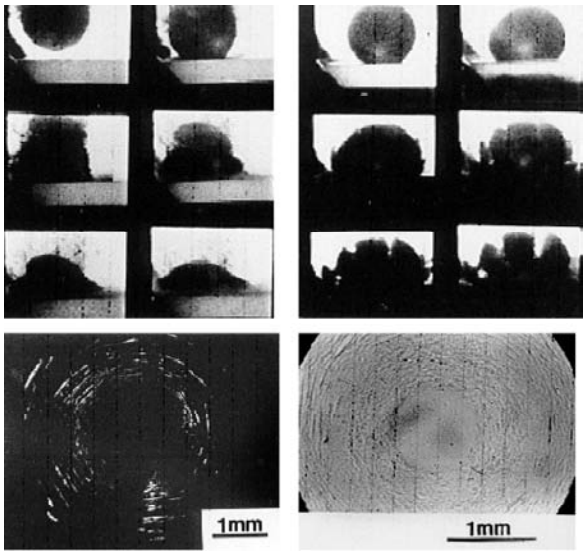

Fig. 3. Left: high-speed sequences (upper) and surface damage (below) for an ice ball impacted onto a PMMA plate (Interframe time 20 μs), Right: high-speed sequences (upper) and surface damage (below) for a nylon ball impacted onto a PMMA plate (Interframe time 20 μs).

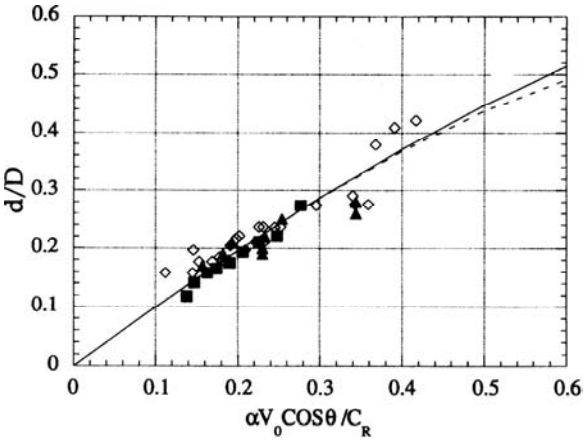

Fig. 4. Comparisons between the theoretical predictions (solid line by Eq. (3.17a) and dot line by Eq. (3.17b) and the experimental data for the undamaged diameters on PMMA plates impacted by ice balls (◊), water drops (■) and nylon balls (▲), as a function of effective impact velocity of projectile.

leftward simultaneously. The X_B is a stationary discontinuity surface with regard to the obverse plastic strain. It is worthwhile to notice that the reflected elastic wave *BC* will play an unloading role with regard to the incident plastic unloading wave *TC*. Caused by the interaction of the unloading plastic wave *TC* and the reflected unloading elastic wave *BC* at X_C another stationary strain-discontinuity X_C appears, which is nearer the front surface and is a stationary discontinuity surface with regard to the reverse plastic strain. More details can be found in [11].

From our analysis it is shown that, only because of the plastic unloading (reverse yield) effect and consequently the existence of stationary discontinuity surfaces X_B and X_C, the tensile stress zone can be formed near the front surface where the impulsive compressive load is applied, and the corresponding particle velocity becomes negative.

Once the tensile stress is larger than the critical tensile stress of the concerned material, particularly for the brittle materials with lower tensile strength or with pre-cracks, the so-called front spalling may occur, another form of dynamic unloading failure. This may be of significance in the study of dynamic fracture for materials/structures under explosion/impact loading, and consequently in the design of setting-up used for anti-explosion/impact.

3.2.2. Surface cracks induced by Rayleigh surface waves

When a plate (target) is impacted by a sphere (projectile), two regions will be formed in both the sphere and the plate in such a non-planar impact, namely, a “contact region” when the expanding contact edge travels at a velocity in excess of all of the stress waves and thus the stress wave effects are covered up and restrained, and a “non-contact region” when the stress waves pass ahead of the expanding contact edge and thus the unloading waves play a dominant role. The theoretical analyses for such phenomenon studied by predecessors [15,16] are limited to the situation of a rigid target impacted by a non-rigid sphere. More general and actual situation of a non-rigid target impacted by a non-rigid sphere was first time studied in [17].

Based on analyses of stress wave propagation, we illustrate that it is the unloading Rayleigh waves which induce tensile stresses and consequently the corresponding ripple surface deformation and the annular damaged region with many short circumferential surface cracks on the non-contact surface region, as shown by the experimental results given in Fig. 3. Theoretically such phenomenon is first time reasonably explained; and experimentally high velocity erosion tests of plate impacted by ice sphere are first time successfully completed.

Starting from such an analysis based on the unloading Rayleigh surface wave propagating in the velocity of C_R, taking account of the wave impedance difference between the non-rigid projectile and the non-rigid target, it is found that the critical radius of the undamaged circle on the non-rigid target, r_{cr}

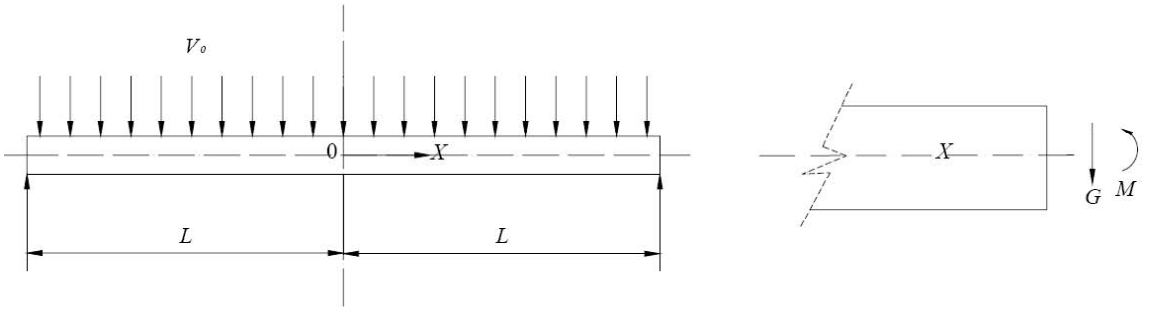

Fig. 5. Simple supported beam with length 2*L* subjected to a uniformly distributed impulsive velocity V_0.

(=*d*/2), can be described by the following non-dimensional equation:

$$\frac{r_{cr}}{R}=\frac{d}{D}=\frac{V}{C_R}\left[1+\left(\frac{V}{C_R}\right)^2\right]^{-1/2},$$

$$V=\frac{V_0}{2}\left[1+\frac{(\rho C)_{tar}}{(\rho C)_{pro}+(\rho C)_{tar}}\right], \qquad (3.17a)$$

or approximately when $V/C_R \le 0.6$:

$$\frac{r_{cr}}{R}=\frac{d}{D}=\frac{V}{C_R}\left[1-\frac{1}{2}\left(\frac{V}{C_R}\right)^2\right],$$

$$V=\frac{V_0}{2}\left[1+\frac{(\rho C)_{tar}}{(\rho C)_{pro}+(\rho C)_{tar}}\right], \qquad (3.17b)$$

$$\text{for } \frac{V}{C_R}\le 0.6,$$

where $R = D/2$ is the radius of the projectile, C_R the Rayleigh surface wave velocity, V_0 the impact velocity of the projectile and ρC the wave impedance for projectile (if with subscript "pro") and target (if with subscript "tar"). For projectile angle-impact onto target, the above equations are still held, if $V\cos\theta$ is used instead of V and the impact angle θ is defined as the angle between the impact line and the normal line of target plane.

The comparisons between our experimental results for both ice sphere erosion and nylon sphere erosion and the theoretical predictions of both Eq. (3.17a) denoted by solid line and Eq. (3.17b) denoted by dashed line are shown in Fig. 4. In the same figure, the experimental data reported by others for ice ball angle-impact and water drop impact [18-20] are also plotted. The satisfactory agreement between the non-dimensional theoretical predictions and the numerous experimental results shown in the figure fully proves that the erosion of target impacted by projectiles of different materials such as hail, water drop and nylon sphere can be satisfactorily described by the unified non-dimensional Eq. (3.17) proposed.

3.2.3. Dynamic failure of beams under transverse impact

Researches reported in the literatures on the dynamic failure of beams under transverse impact indicated that three basic failure modes may exist, namely, large ductile deformations (Mode I), tensile-tearing (Mode II), and transverse shearing (Mode III) [21]. The former two modes are mainly resulted from bending wave propagation, while the third one is closely related to the transverse shear wave propagation [11].

Most literatures were mainly focused on the failure due to large deflection (Mode I) and tensile tearing (Mode II). It is Nonaka who introduced the so-called plastic shearing hinge (slide) to study the dynamic shear response of beams (Mode III), although it was limited to the simplest rigid-perfectly plastic beams and consequently the plastic shearing hinge is limited to a stationary singular surface [22]. The Nonaka's model is usually regarded as a classic solution, but theoretically it does not satisfy the requirement that the kinematics consistency condition and the dynamic consistency condition across a shearing hinge (a singular surface) should be simultaneously satisfied. In order to deep the understanding on the shear failure mode (Mode III), rigorously based on the theory of stress wave propagation, taking account of material strain hardening, we established a more comprehensive shear failure theory in terms of "traveling plastic shearing hinge" [13]. The basic characters of a traveling plastic shearing hinge in a beam are in first time studied. For a rigid-linear hardening plastic beam, it is shown that the traveling velocity of a plastic shear hinge C_Q is invariable, $C_Q=\sqrt{G_p/m}$, where G_p is the linear hardening modulus of shear force (Q) versus shear strain (γ) curve and m the linear density of beam.

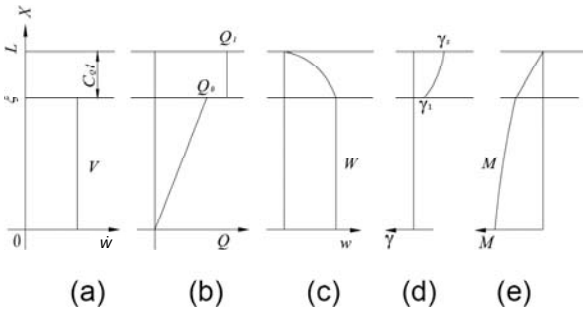

Fig. 6. Simply supported beam subjected to impulsive loading at time $t<T_s$, (a) transverse velocity profile, (b) shear force distribution, (c) transverse displacement profile, (d) shear strain distribution, (e) bending moment distribution.

For a simply supported beam loaded impulsively, as shown in Fig. 5, the analytic solutions for the dynamic transverse displacement w, transverse velocity $\dot{w}$, transverse shear force Q, transverse shear strain γ, transverse shear strain-rate $\dot{\gamma}$ as well as bending moment M are completely obtained as functions of X and t respectively.

At the time $t>0$, when the traveling plastic shearing hinge which is initiated at $X = L$ and $t = 0$, arrives at the transient location $X = \xi$ ($=C_Q t$), the distributions of $\dot{w}$, Q, w, γ, and M with respect to X are shown in Fig. 6, respectively.

As can be seen from Fig. 6, the traveling plastic shearing hinge is a strong discontinuity propagating with velocity C_Q, across which jumps of transverse velocity $[\dot{w}]$, transverse shear force $[Q]$ and transverse shear strain $[\gamma]$ exist. As to the shear force discontinuity, it is a jump from the yield shear force Q_0 to Q_1 ($>Q_0$). Our research transpires that, as described by the following Eq. (3.18), the shear force behind the traveling hinge Q_1 decreases with t, since the length of plastic zone, $l_s = C_Q t$, is less than L:

$$Q_1(t) = mC_Q V_0 + Q_0\left[1+\ln\left(1-\frac{C_Q t}{L}\right)\right] = Q_s + Q_0 \ln\left(1-\frac{C_Q t}{L}\right), \tag{3.18}$$

where $Q_s = Q_0 + mC_Q V_0$ is the maximum value of $Q_1(t)$ at $t = 0$. The decrease of $Q_1(t)$ with time means that the beam segment behind the traveling plastic shear hinge ($\xi \le X \le L$) is in a unloading state, which leads to a non-uniform distribution of plastic shear strain as shown in Fig. 6d. Thus the final failure of beam is closely related to such an unloading process.

It is easy to approve that the classic Nonaka's solution is only an approximate solution of our analysis when the dimensionless length of the final plastic region $\bar{L}_s$ ($=L_s/L$, where L_s the final length of shear plastic zone) approaches zero ($\bar{L}_s \cong 0$).

Moreover, in addition to the conventional failure modes of excess deflection failure and excess shear strain failure, a new shear failure mode due to adiabatic shearing is proposed. In other words, there basically exist three possible failure modes: (1) excess transverse deflection failure mode when the transverse displacement w_f exceeds the critical transverse displacement w_c allowed in design ($w_f \ge w_c$); (2) excess shear strain failure mode when the maximum shear strain γ_s exceeds the critical shear strain γ_c allowed in design, which is usually strain-rate sensitive ($\gamma_s \ge \gamma_c$); (3) adiabatic shear failure mode when a certain critical adiabatic shearing (thermo-viscoplastic instability) criterion is satisfied, which is generally dependent on both strain and strain-rate under a certain temperature. This mode of failure is attributed to the highly localized shear deformation within a so called "adiabatic shear band" which leads to the final adiabatic shear failure. In mechanism, it is related to the balance between the stress drop due to thermal softening by adiabatic heating ($\partial\tau/\partial T < 0$, where τ is the shear stress and T the temperature) and the stress rise due to strain hardening ($\partial\tau/\partial\gamma > 0$) and strain-rate hardening ($\partial\tau/\partial\dot{\gamma} > 0$) of a material, namely the so-called thermo-viscoplastic constitutive instability of a material. The critical condition can be described by a corresponding strain-strain rate-temperature dependent adiabatic shear failure criterion established by us [23,24], of which more details will be further discussed in the below Section 5.

4. NON-LINEAR VISCOELASTIC MATERIAL MODEL AND VISCOELASTIC WAVES

The wave propagations intimately relate to the material behavior. In fact, without knowing the dynamic constitutive relation of materials under high strain rates, no wave propagation can be correctly analyzed; and the characters of wave propagation actually reflect the characters of materials.

Since the well-known J. Hopkinson's dynamic experiment in 1872 [25], it was found that the material behavior under impact loading is markedly different from that under quasi-static loading. This knowledge from experimental investigations was mainly restricted to metals in the earlier time. After being one of most important engineering materials,

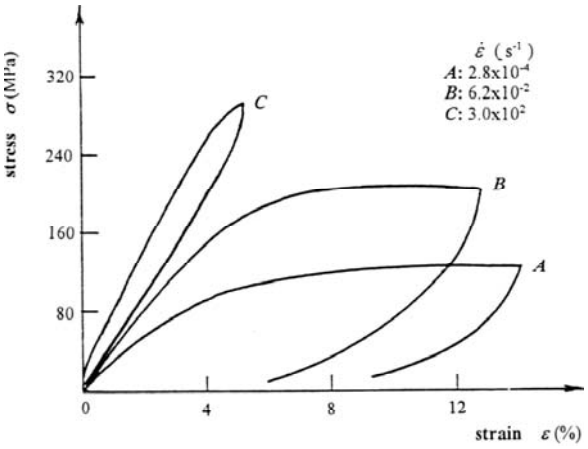

Fig. 7. Experimental σ-ε curves for PMMA.

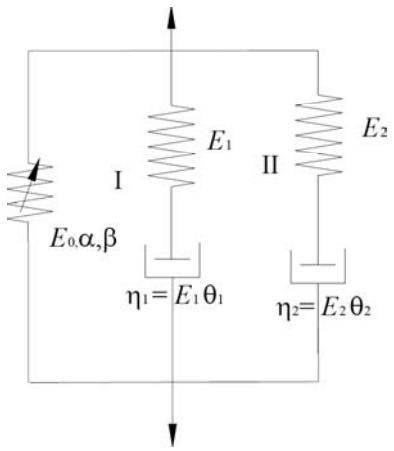

Fig. 8. Rheological model of Eq. (4.1).

polymers or plastics have been studied as the quintessence of viscoelastic materials by many scientists. However, the main parts of those researches have been concentrated in the linear viscoelastic behavior of polymers within low strain rates. In the recent more than twenty years, the dynamic behavior of polymers has been as one of our research directions. For a variety of polymers extensively used in industries, such as polymethy1 methacrylate (PMMA), polycarbonate (PC), polyamide (PA or Nylon), acrylonitrile-butadiene-styrene (ABS), Polybuthylene terephthalate (PBT), epoxy and phenolics thermoset plastics, and the related polymer-matrix composites, their dynamic nonlinear behaviors under a wide strain-rate range of 10^{-4} to 10^{3} s^{-1} have been studied in detail. The results show that the dynamic behavior of polymers can be modeled by a "weak non-linear thermo-viscoelastic constitutive relation", composed of non-linear elasticity and linear viscoelasticity [26]. This material model can be much easier and simpler used to deal with many engineering problem, and to solve the problems of non-linear viscoelastic wave propagations as will be discussed in detail in the following.

4.1. Weak non-linear viscoelastic constitutive model of solids

The experimental investigation by Zhu, Wang and their co-workers for a variety of polymers transpired that the dynamic behavior of polymers is highly sensitive to strain rates, as shown in Fig. 7 for PMMA as an example, and the nonlinear viscoelastic behavior in one-dimensional (1-D) stress state for all the polymers studied can be well described by the following nonlinear viscoelastic constitutive equation, which is sometimes called ZWT model for short [26-28].

$$\sigma = f_e(\varepsilon) + E_1\int_0^t \dot{\varepsilon}\exp\left(-\frac{t-\tau}{\theta_1}\right)d\tau + E_2\int_0^t \dot{\varepsilon}\exp\left(-\frac{t-\tau}{\theta_2}\right)d\tau, \tag{4.1a}$$

$$f_e(\varepsilon) = E_0\varepsilon + \alpha\varepsilon^2 + \beta\varepsilon^3, \text{ or} \tag{4.1b}$$

$$f_e(\varepsilon) = \sigma_m\left[1-\exp\left(-\sum_{i=1}^{n}\frac{(m\varepsilon)^i}{i}\right)\right], \tag{4.1c}$$

where σ, ε and $\dot{\varepsilon}$ are stress, strain and strain rate respectively, the first term $f_e(\varepsilon)$ describes the nonlinear elastic response; the next integral term describes the linear viscoelastic response at low strain rates, in which E_1 and θ_1 are the elastic constant and relaxation time of the corresponding Maxwell element I, respectively; and the last integral term describes the linear viscoelastic response at high strain rates, in which E_2 and θ_2 are the elastic constant and relaxation time of the corresponding Maxwell element II, respectively. As to the first nonlinear elastic term $f_e(\varepsilon)$, it can be described by either Eq. (4.1b) in power polynomial form, where E_0 denotes the initial elastic modulus and α, β are nonlinear elastic constants, or by Eq. (4.1c) in exponential form, where σ_m denotes the asymptotic maximum, *m* the ratio of E_0 and σ_m, and the positive integer *n* is a material parameter characterizing the initial linearity [28]. The corresponding rheological model is shown in Fig. 8. Combined with

micromechanical analysis, Eq. (4.1) can be used to describe the viscoelastic behavior of polymer-matrix composites [29,30].

The nonlinear viscoelastic parameters experimentally determined for typical polymers are given in Table 2.

Theoretically, Eq. (4.1) can be deduced from Green-Revlin multiple-integral constitutive theory [31], or from Coleman-Noll finite linear viscoelastic model [32,33].

To explain why θ_1 is responsible for the viscoelastic behavior at low strain rates while θ_2 is responsible for that at high strain rates, we introduce a new concept of "effective influence domain" of material relaxation time [34]. Considering a simple Maxwell element with elastic modulus E_j and relaxation time θ_j, (or the corresponding viscosity coefficient $\eta_j = E_j\theta_j$), we have the following constitutive relation

$$\dot{\varepsilon} = \frac{\dot{\sigma}_j}{E_j} + \frac{\sigma_j}{\eta_j}. \tag{4.2}$$

At constant strain-rate ($\dot{\varepsilon}$ = const. and $\varepsilon = \dot{\varepsilon} t$), the stress relaxation response σ_j is given by

$$\sigma_j = E_j\theta_j\dot{\varepsilon}\left\{1 - \exp\left(-\frac{\varepsilon}{\theta_j\dot{\varepsilon}}\right)\right\}. \tag{4.3}$$

Consider two extreme cases: when $\dot{\varepsilon}$ approaches infinity σ_j approaches its maximum which is the instantaneous response $\sigma_I = E_j\varepsilon$, and when $\dot{\varepsilon}$ approaches zero σ_j approaches its minimum which is the equilibrium response $\sigma_E = 0$. By introducing the non-dimensional stress relaxation response defined as

$$\bar{\sigma}_j = \frac{\sigma_j}{\sigma_{max} - \sigma_{min}} = \frac{\sigma_j}{\sigma_I - \sigma_E} = \frac{\sigma_j}{E_j\varepsilon},$$

Eq. (4.3) can be rewritten in a non-dimensional form:

$$\bar{\sigma}_j = \frac{\theta_j\dot{\varepsilon}}{\varepsilon}\left\{1 - \exp\left(-\frac{\varepsilon}{\theta_j\dot{\varepsilon}}\right)\right\} = \frac{\theta_j}{t}\left\{1 - \exp\left(-\frac{t}{\theta_j}\right)\right\}, \tag{4.4}$$

To define a Effective Influence Domain (EID) of θ_j, we regard $\bar{\sigma}_j = 0.995$ as the beginning of a relaxation process and $\bar{\sigma}_j = 0.005$ as the end of this relaxation process, then the EID of θ_j in terms of time t can be easily determined from Eq. (4.4)

$$10^{-2} \le \frac{t}{\theta_j} \le 10^{2.3}, \tag{4.5a}$$

or, in terms of strain rate when assume $\varepsilon = 1$,

$$10^{2} \ge \frac{\dot{\varepsilon}}{\left(\frac{\varepsilon}{\theta_j}\right)} \ge 10^{-2.3}. \tag{4.5b}$$

It means that the EID for any relaxation time θ_j is about 4.5 orders of magnitude in either time scale or strain-rate scale. As can be seen from Table 2, θ_1 is generally of the order of 1 to 10^2 s, while θ_2 is of the order of 10^{-6} to 10^{-4} s, namely, θ_1 is of the order of 10^5 to 10^7 times higher than θ_2. This means that each of them exerts its influence in its own dominant range of strain rates, and is responsible for the viscoelastic behavior at low strain rates and high strain rate respectively.

It is worthwhile to emphasize that only the "loading-and-unloading" behavior of a material is comprehensively understood, as shown in Fig. 7, can its constitutive character be determined. In fact, it is impossible to distinguish the non-linear elasticity, elasto-plasticity or viscoelasticity based on the loading stress-strain curves only. The

Table 2. The typical nonlinear viscoelastic parameters experimentally determined [26].

	Epoxy	PMMA-1	PMMA-2	PMMA-3	PC
ρ_o, kg/m^3	1.20x10^3	1.19 x10^3	1.19 x10^3	1.19 x10^3	1.20 x10^3
E_0, GPa	1.96	2.05	2.19	2.95	2.20
α, GPa	4.12	4.71	4.55	10.9	23
β, GPa	-181	-233	-199	-96.4	-52
E_1, GPa	1.47	0.897	0.949	0.832	0.10
θ_1, s	157	15.3	13.8	7.33	470
E_2, GPa	3.43	3.07	3.98	5.24	0.73
θ_2, ms	8.57	95.4	67.4	40.5	140

unloading behavior of polymers in the strain rate range of 10^{-4}~10^{3} s^{-1} is firstly considered and experimentally measured by our research group, and based on those experimental data the constitutive Eq. (4.1) was proposed.

Referring to ZWT Eq. (4.1), the following constitutive characters should be especially emphasized:

1. The physical or constitutive non-linearity only comes from the pure elastic equilibrium response $f_e(\varepsilon)$, while all the rate/time dependent responses are essentially linear and consequently can be still described by linear viscoelastic elements even when the apparent, overall response is nonlinear. Such a constitutive non-linearity may be termed the "rate- independent non-linearity" - a kind of weak non-linearity. Then it provides a possibility of generalizing what has been established in linear viscoelasticity to the rate-dependent response of ZWT materials without substantial difficulties.
2. According to the experimental results obtained for a variety of polymers [26,35], the order of magnitude of α/E_0 is 10^0~10^1, while the order of magnitude of β/E_0 is 10~10^2. This means that the non-linear elastic response can be ignored when ε<0.01.
3. Since the EID for any relaxation time θ_j is about 4.5 orders of strain-rate and the order of magnitude of θ_2 is about 10^{-6}-10^{-4} s as shown in Table 2, under quasi-static loading (the time scale is about 1~10^2 s) Maxwell element II with relaxation time θ_2 is completely relaxed. Consequently Eq. (4.1) becomes:

$$\sigma = f_e(\varepsilon) + E_1 \int_0^t \dot{\varepsilon}(t) \exp\left(-\frac{t-\tau}{\theta_1}\right) \mathrm{d}\tau. \qquad (4.6)$$

4. Since the EID for any relaxation time θ_j is about 4.5 orders of strain-rate and the order of magnitude of θ_1 is about 1-10^2 s as shown in Table 4-1, under dynamic loading, (the time scale is about 1~10^2 μs), Maxwell element I with relaxation time θ_1 is not relaxed any more, so that its response is only described by a spring. Thus, Eq. (4.1) becomes:

$$\sigma = f_e(\varepsilon) + E_1\varepsilon + E_2 \int_0^t \dot{\varepsilon}(t) \exp\left(-\frac{t-\tau}{\theta_2}\right) \mathrm{d}\tau = \sigma_e(\varepsilon) + E_2 \int_0^t \dot{\varepsilon}(t) \exp\left(-\frac{t-\tau}{\theta_2}\right) \mathrm{d}\tau. \qquad (4.7)$$

Furthermore, in the case of ε<1%, $\sigma_e(\varepsilon)$(=$f_e(\varepsilon) + E_1\varepsilon$) reduces to $(E_0+E_1)\varepsilon$, thus the above equation reduces to a linear viscoelastic relation

$$\sigma = (E_0 + E_1)\varepsilon + E_2 \int_0^t \dot{\varepsilon}(t) \exp\left(-\frac{t-\tau}{\theta_2}\right) \mathrm{d}\tau = E_{eff}\varepsilon + E_2 \int_0^t \dot{\varepsilon}(t) \exp\left(-\frac{t-\tau}{\theta_2}\right) \mathrm{d}\tau. \qquad (4.8)$$

This is rheologically equivalent to the well-known three-element standard linear solid model.

Undoubtedly, the proposed one-dimensional (1-D) nonlinear viscoelastic model (or called visco-hyperelastic model) must be developed to three-dimensional model for the need of numerical simulations. For instance, rubbers and foams are widely used as vibration isolators and cushioning material between neighboring components to mitigate impact loads arising from accidental drops. For effective shock amelioration, the mechanical properties of those materials have to be determined for a spectrum of strain rates undergoing very large deformation which results in non-linear rate-dependent constitutive response. Thus, the 1-D weak non-linear viscoelastic model should further be developed. Based on the experiments and theoretical analysis, assuming that the material is incompressible, a three-dimensional (3-D) visco-hyperelastic model has been proposed [36,37], which is incorporated into a finite element code (DYNA3D) and employed in the 3-D impact response simulation. The numerical results exhibit good agreement with experimental data, demonstrating that the model is suitable for prediction of visco-hyperelastic behavior in 3-D situations, even though the parameters in the model are determined from uni-axial tests.

4.2. Weak non-linear thermo-viscoelastic constitutive model of solids

The previously proposed weak nonlinear viscoelastic constitutive model can be further generalized to include temperature effect. Such a weak nonlinear thermo-viscoelastic constitutive model has been further developed by us, taking account of the equivalent relation between rate dependency and temperature dependency [34,35,38].

The equivalent relation between rate/time-dependency and temperature dependency for polymeric materials is an important research problem. A number of studies on thermo-viscoelastic constitutive relations and the related temperature rate/time equivalence have been conducted. For linear viscoelastic materials, it has been found [39]

that by introducing the so-called "shift factor" $a_l(T)$ and the related "reduced time",

$$t_l = \frac{t}{a_l(T)}, \tag{4.9}$$

a group of relaxation moduli or creep compliances at different temperatures T may be reduced to a unified function at a reference temperature T_R with a single argument t_l. A material with such a character is called thermo-rheologically simple material [40].

Stating from the ZWT weak nonlinear viscoelastic constitutive model, by assuming that the material parameters in ZWT equation all are functions of temperature T, and introducing a "non-dimensional relaxation time" $a(T)$ defined as $a(T) = (\theta(T))/(\theta_R(T)) = (\eta(T)E_R)/(\eta_R E(T))$ and a "over stress" defined as $(\sigma - \sigma_e(T,\varepsilon))$ or a "non-dimensional over stress" $\bar{\sigma}$ defined as $\bar{\sigma} = (\sigma - \sigma_e(T,\varepsilon))/(E(T))$, Eq. (4.7) under high strain rate then can be re-written as:

$$\bar{\sigma}=\frac{\sigma-\sigma_e\left(T,\varepsilon(\tau)\right)}{E_2}=\int_0^t \dot{\varepsilon}(t)\exp\left(-\frac{t-\tau}{\theta_2}\right)\mathrm{d}\tau= \int_0^t \exp\left(-\frac{t_R-\tau_R}{\theta_R}\right)\frac{\mathrm{d}\varepsilon}{\mathrm{d}\tau_R}\mathrm{d}\tau_R, \tag{4.10}$$

where θ_R, E_R, and η_R are the relaxation time, the elastic constant and the viscosity coefficient at the reference temperature, respectively, and similar to Eq. (4.9) a "reduced time" defined as $t_R=t/a(T)$ has been introduced in the right side of the second equal sign. From Eq. (4.10) it can be seen that if the thermo-viscoelastic response of polymers is described by the non-dimensional over stress $\bar{\sigma}$, then the only independent variable is the reduced time t_R. In other words, the $\bar{\sigma}$- t_R curves at different temperatures are coincident with each other, if their strain-history with regard to the reduced time, $\varepsilon(t_R)$, are same. Thus Eq. (4.10) characterizes the "time-temperature equivalence" for polymers at high strain rates and large deformations.

Moreover, by introducing the following non-dimensional parameter

$$Z = \dot{\varepsilon}\theta_2(T), \tag{4.11}$$

the "reduced strain rate" $d\varepsilon/dt_R$ is then related to the Z by the following equation:

$$\frac{\mathrm{d}\varepsilon}{\mathrm{d}t_R} = a(T)\frac{\mathrm{d}\varepsilon}{\mathrm{d}t} = \frac{\dot{\varepsilon}\theta(T)}{\theta_R} = \frac{Z}{\theta_R}. \tag{4.12}$$

So, the non-dimensional parameter Z is physically corresponding to the "reduced strain rate", since θ_R is a given constant. It is worthwhile to note that most experiments are preferred to conduct under constant temperature and constant strain rate. Under such conditions, Eq. (4.10) becomes

$$\frac{\bar{\sigma}_\tau}{Z} = 1-\exp\left(-\frac{\varepsilon}{Z}\right). \tag{4.13}$$

It means that the description of rate-dependence and temperature-dependence of overstress-strain relation can be unified in terms of single parameter Z. In other words, Z characterizes the quantitative equivalence between $\dot{\varepsilon}$ -dependence and T-dependence. For example, when T increases, $\theta(T)=\eta(T)/E(T)$ decreases in general, and consequently Z decreases if $\dot{\varepsilon}$ = const.; this is equivalent to decrease the strain rate if T = const. Graphically, it corresponds to a shift of overstress-strain rate curve along the positive strain-rate-axis.

4.3. Viscoelastic wave propagation in non-linear viscoelastic bars

The governing equations for longitudinal nonlinear viscoelastic waves propagating in a thin bar are constituted by the following equations, i.e., the motion equation and the continuity equation,

$$\rho_0\frac{\partial v}{\partial t} = \frac{\partial \sigma}{\partial X},\quad \frac{\partial v}{\partial X} = \frac{\partial \varepsilon}{\partial t}, \tag{4.14a,b}$$

and a constitutive equation, where v denotes the particle velocity. For a ZWT material, of which behavior is modeled by ZWT Eq. (4.1), its constitutive equation in an equivalent differential form under dynamic loading can be written as (see Eq. (4-7)

$$\frac{\partial \sigma}{\partial t}+\frac{\sigma}{\theta_2} = \left[\sigma_e'(\varepsilon)+E_2\right]\frac{\partial \varepsilon}{\partial t}+\frac{\sigma_{eff}(\varepsilon)}{\theta_2}, \tag{4.14c}$$

By means of the well-known characteristics method [11], the above partial differential equations are equivalent to three sets of ordinary differential equations, each set consisting of a characteristics equation and a corresponding compatibility condition along the characteristics. The first two sets of characteristics and their compatibility equations are

$$dX=\pm C_V\,\mathrm{d}t,\ dv=\pm\frac{1}{\rho_0 C_V}\mathrm{d}\sigma\pm\frac{\sigma-\sigma_e(\varepsilon)}{\rho_0 C_V\theta_2}\mathrm{d}t= \pm\frac{1}{\rho_0 C_V}\mathrm{d}\sigma+\left[\frac{\sigma-\sigma_e(\varepsilon)}{\left(\sigma_e'+E_2\right)\theta_2}\right]\mathrm{d}X, \tag{4.15}$$

where the positive sign is for rightward waves, the negative sign for leftward waves, and C_V the wave velocity along the characteristics:

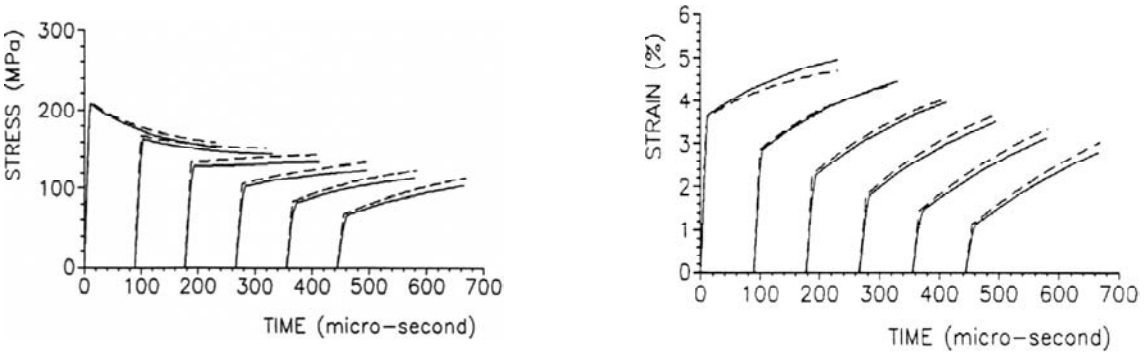

Fig. 9. Nonlinear viscoelastic waves in PMMA bar under constant-velocity (80 m/s) impact condition, showing (a) stress profiles and (b) strain profiles, at *X*=0, 0.2, 0.4 0.6, 0.8, 1.0 m, respectively.

$$C_V = \sqrt{\frac{1}{\rho_0}\left(\sigma_e' + E_2\right)} = \sqrt{\frac{f_e'(\varepsilon) + E_1 + E_2}{\rho_0}}. \quad (4.16)$$

The third set corresponds to the relation along the particle motion locus and consists of

$$\mathrm{d}X = 0, \quad \mathrm{d}\varepsilon - \frac{\mathrm{d}\sigma}{\sigma_e' + E_2} - \frac{\sigma - \sigma_e(\sigma)}{\sigma_e' + E_2}\frac{\mathrm{d}t}{\theta_2} = 0. \quad (4.17)$$

It is worthwhile to note from the compatibility condition Eqs. (4.15b) and (4.17b) that the high frequency relaxation time θ_2 always appears in the terms with *dt* (or *dX*), and in a form of $(\sigma - \sigma_e)dt/\theta_2$, the dispersion and attenuation of viscoelastic waves are, in fact, described by those terms, and thus mainly depend on θ_2 and the stress difference between the viscoelastic overall stress σ and the pure elastic equilibrium stress σ_e, namely, the stress relaxation process.

In the case of linear viscoelastic wave with strong discontinuity front (shock wave), it is easy to show [11] that the viscoelastic shock wave propagates with the velocity of C_V and attenuates exponentially according to the following equation:

$$\sigma == \sigma^* \exp\left(-\alpha_a X\right),$$
$$\alpha_a = \frac{E_2}{2\theta_2 C_V\left(E_0 + E_1 + E_2\right)} = \frac{\rho_0 C_V}{2\eta_2\left(1 + \dfrac{E_0 + E_1}{E_2}\right)^2}, \quad (4.18)$$

where $\sigma^* = \sigma(0,0)$ and α_a is the attenuation factor.

By using the numerical characteristics method [11], the nonlinear viscoelastic wave propagation in polymer bars can be computationally simulated to study how the nonlinear viscoelastic wave propagation character depends on the constitutive character [41,42]. For instance, the relaxation time θ_2 are known as 95.4 μs for PMMA and 8.57 μs for epoxy, respectively (see Table 2). Under a boundary condition of constant-velocity impact (80 m/s), the typical results of computational simulation are given in Fig. 9 and Fig. 10 for PMMA and epoxy, respectively, including (a) stress profiles and (b) strain profiles at the different distances from the impact boundary (*X* = 0).

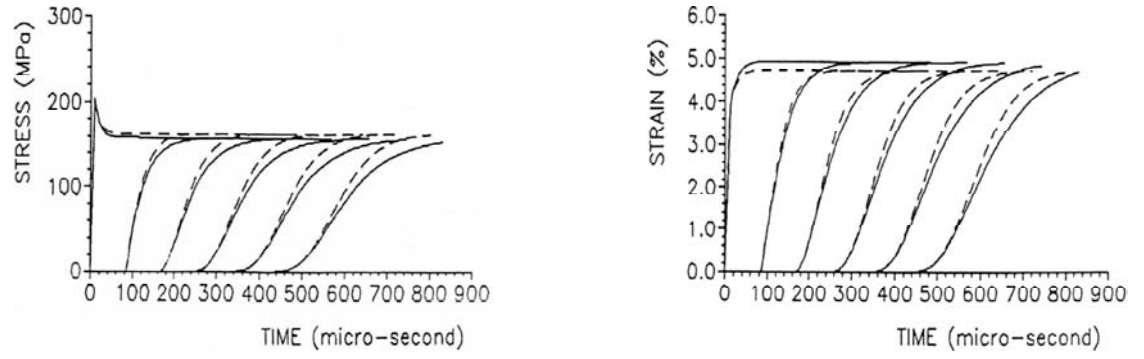

Fig. 10. Nonlinear viscoelastic waves in epoxy bar under constant-velocity (80 m/s) impact condition, showing (a) stress profiles and (b) strain profiles, at *X*=0, 0.2, 0.4 0.6, 0.8, 1.0 m, respectively.

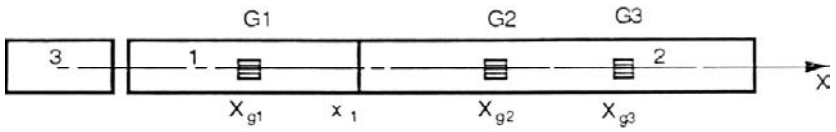

Fig. 11. Schematic of the experimental arrangement 1-incident elastic bar, 2-transmitted viscoelastic bar, 3-elastic striker bar with the same material as bar 1, and G1, G2, and G3 are strain gauges.

The following characters should be especially pointed out from Fig. 9 and Fig. 10.

Firstly, in both the figures, the broken lines are the results of linear model when the non-linear elastic term in Eq. (4.7) is reduced to a linear elastic term ($\alpha = \beta = 0$). As can be seen, the constitutive non-linearity exerts a marked influence on both the wave amplitude and the wave profile shape, and thus the nonlinear effects cannot be neglected in the case of high-velocity large deformation, even the constitutive non-linearity is rate-independent. However, if the strain is small enough, e.g., $\varepsilon < 1\%$, in the present examples, the linear approximation can be accepted since it coincides well with the nonlinear one.

Next, as can be seen from both figures, in contrast with the case in linear elastic waves, no proportional relation exists between the viscoelastic stress wave and strain wave. One of the most distinct characters of viscoelastic waves is that for the waves at and near the impact boundary, the stress profile behind the wave front displays a "stress relaxation-like" character (showing a decrease of amplitude with time), while the strain profile behind the wave front on the contrary displays a "strain creep-like" character (showing an increase of amplitude with time). It implies that the viscoelastic dynamic stress at any position cannot be determined directly from an experimentally measured dynamic strain profile at the same position by simply multiplying with the apparent elastic modulus.

Moreover, all viscoelastic waves attenuate with propagating distance X, regardless of stress waves or strain waves. Comparing with the results in Fig. 9 and Fig.10, it can be seen that the viscoelastic waves in a PMMA bar, of which the θ_2 is higher, show a weaker attenuation. This result is consistent with the theoretical analysis according to Eqs. (4.15) and (4.17), since the viscoelastic wave attenuation is mainly dominated by the term of $[\sigma - \sigma_e(\varepsilon)]/\theta_2$, or in other words, becomes weaker with increasing θ_2.

Furthermore, recall that (a) the constitutive attenuation of viscoelastic waves strongly depends on the high-strain-rate relaxation time θ_2, and (b) each θ has its "effective influence domain" about 4.5 orders of magnitude in either time scale or strain-rate scale, it can be correspondingly expected that with regard to the attenuation of viscoelastic waves, an "effective influence domain" either in terms of time or in terms of distance should exist for a given θ_2 [41,42]. In other words, an "effective influence time (EIT) $t_{eff} = \theta_2$, or an "effective influence distance (EID) $X_{eff} = C_V \theta_2$ can be defined, respectively, to characterize the time and the propagation distance effectively dominated by θ_2. Once $t > t_{eff}$ or $X > X_{eff}$, the relaxation process of viscoelastic wave propagation will be no longer influenced by θ_2. According to Fig. 9 and Fig. 10, it can be determined that $X_{eff} = 0.214$ m for PMMA and $X_{eff} = 0.0205$ m for epoxy, respectively.

4.4. Determining dynamic constitutive relationship based on the viscoelastic wave propagation

Starting from the proposed weak nonlinear viscoelastic constitutive model, a new method to experimentally determine the dynamic behavior of viscoelastic material is proposed [43], which is based on the characters of viscoelastic wave propagation. The crux is how to experimentally determine the high strain-rate parameters E_2 and θ_2 of the tested polymer, since other parameters can be rather easily determined by quasi-static tests, as discussed in the deducing of Eq. (4.7).

Basically, the technique consists of two long bars, the incident elastic bar-1 and the transmitted viscoelastic bar-2, as shown in Fig. 11. The incident elastic bar and the elastic projectile-3 are made of the same elastic material, of which the density ρ_{el} and Young's modulus E_{el} are known, and consequently the elastic wave velocity $C_0=(E_{el}/\rho_{el})^{1/2}$ and the wave impedance $\rho_{el}C_0$ of the elastic incident bar are known. The transmitted viscoelastic bar is made of the polymer to be tested and its density ρ_v is known.

When the projectile with velocity V_0 impacts onto the incident bar, a trapezoidal strain pulse $\varepsilon_i(X,t)$ is recorded by the strain gage G_1 mounted on the incident bar, and according to the wave propagation theory [11], the amplitude of incident stress wave σ_i

can be determined either by the measured impact velocity V_0, namely $\sigma_i = -\rho C_0 V_0/2$, or by the incident strain ε_i measured by the strain gauge G_1 at X_{g1}, namely $\sigma_i = E_{el}\varepsilon_i$.

When the incident wave arrives the interface ($X = X_1$) between the incident bar and transmitter bar, a reflected elastic wave $\varepsilon_r(X,t)$ and a transmitted viscoelastic wave $\varepsilon_t(X,t)$ are generated. Because of that the stress on the both sides of the interface should be the same, the transmitted stress $\sigma_t(X_1,t)$ on the interface, which propagates with velocity C_v into viscoelastic bar, can be calculated from the measured incident wave $\varepsilon_i(X,t)$ and reflected wave $\varepsilon_r(X,t)$ propagating in elastic bar,

$$\sigma_t\left(X_1,t\right) = E_{el}\left[\varepsilon_i\left(X_1,t\right) + \varepsilon_r\left(X_1,t\right)\right]. \qquad (4.19a)$$

Once the $\sigma_i(X_1,t)$ and $\sigma_t(X_1,t)$ on the interface are obtained, according to the reflection and transmission principle for strong discontinuity waves [11], the instantaneous wave impedance $\rho_V C_V$ of viscoelastic bar and the corresponding wave velocity C_V can be determined by the following equations:

$$\rho_v C_V = \frac{\sigma_t\left(\rho_{el}C_0\right)}{2\sigma_i - \sigma_t}, \text{ and}$$
$$C_V = \frac{\sigma_t\left(\rho_{el}C_0\right)}{\rho_v\left(2\sigma_i - \sigma_t\right)}. \qquad (4.19b)$$

Recalling the definition of C_V in Eq. (4-16), in the case of linear viscoelastic waves, the high strain rate elastic constant E_2 can be determined:

$$E_2 = \rho_0 C_V^2 - \left(E_0 + E_1\right). \qquad (4.20)$$

Now it becomes clear that the incident elastic bar in the present experiment plays not only a role of transferring loading to the viscoelastic specimen (transmitted bar), but also provides a tool to measure the transmitted stress $\sigma_t(X_1,t)$ at the bar-specimen interface through the recorded incident wave $\varepsilon_i(X,t)$ and reflected wave $\varepsilon_r(X,t)$, and consequently the instantaneous wave impedance $\rho_V C_V$ and the high strain rate elastic constant E_2 of viscoelastic specimen.

The next step is how to determine the high strain rate relaxation time θ_2. Recalling the definition of the attenuating factor α_a in Eq. (4.18b), it is clear that the θ_2 can be deduced from α_a since the other parameters in Eq. (4.18b) now are known, while according to Eq. (4.18a) the α_a can be approximately obtained by the following equation when the viscoelastic strain wave front $\varepsilon_t(X_{g2})$ recorded by strain gauge G_2 and the viscoelastic strain wave front $\varepsilon_t(X_{g3})$ recorded by strain gauge G_3 are measured:

$$\alpha_a = \frac{\ln\left(\varepsilon_t\left(X_{g3}\right)\right) - \ln\left(\varepsilon_t\left(X_{g2}\right)\right)}{X_{g3} - X_{g2}}. \qquad (4.21)$$

Note that the high strain-rate parameters E_2 and θ_2 in the nonlinear viscoelastic equation (4-7) and in the linear viscoelastic equation (4-8) are actually the same. This means that the E_2 and θ_2 determined in linear situation (e.g. ε <1%) should still be valid in nonlinear situation (e.g. ε >1%).

As a typical example, experiments were performed by using an incident bar made of aluminum alloy and a transmitter bar made of PMMA [43]. From quasi-static tests, the related parameters are known as: E_0 = 70.5 GPa, ρ_{el} = 2.7 g/cm^3, and C_0 = 5110 m/s for the aluminum alloy, and $E_a = E_0 + E_1$=2.82 GPa and ρ_v = 1.19 g/cm^3 for the PMMA.

Then, according to the present dynamic experimental technique schematically shown in Fig. 11, by measuring the $\varepsilon_i(X_{g1},t)$, $\varepsilon_r(X_{g1},t)$, $\varepsilon_t(X_{g2},t)$ and $\varepsilon_t(X_{g3},t)$, the C_V and α_a, and subsequently the high strain-rate parameters E_2 and θ_2 for the tested PMMA are determined as:

$$C_V = 2.22 \text{ km/s}, \ \alpha_a = 0.103 \text{ m}^{-1},$$
$$E_2 = 3.04 \text{ GPa}, \ \theta_2 = 1135 \ \mu\text{s}. \qquad (4.22)$$

The transmitted viscoelastic strain waves measured at X_{g2} and X_{g3}, $\varepsilon_t(x_{g2},t)$ and $\varepsilon_t(x_g,t)$, are given in Fig. 12a, showing the creep-like strain profile and the attenuation of viscoelastic waves. In the same figure, the theoretical prediction of $\varepsilon_t(x_{g3},t)$ is also given (in solid line) for comparison, which is calculated from the measured $\varepsilon_t(x_{g2},t)$ by the numerical characteristics method as solving a direct problem.

On the other hand, from the elastic incident strain wave $\varepsilon_i(X_{g1},t)$ and the reflected elastic strain wave $\varepsilon_r(X_{g1},t)$ measured at X_{g1}, the transmitted stress $\sigma_t(X_1,t)$ on the interface can be determined as experimental curve (in dashed line) shown in Fig. 12b. In the same figure, the theoretical prediction of $\sigma_t(X_1,t)$ is also given (in solid line) for comparison, which is calculated from the measured $\varepsilon_t(x_{g2},t)$ by the numerical characteristics method as solving an inverse problem.

As can be seen from the Figs. 12a and 12b, the theoretical predictions are in good agreement with the experimental results in the both situations. Thus, the validity of the proposed method is confirmed.

It is worthwhile to emphasize again that any approximate treatment of viscoelastic polymer as an elastic material will lead to a serious error particularly in regard to the wave propagation. In fact,

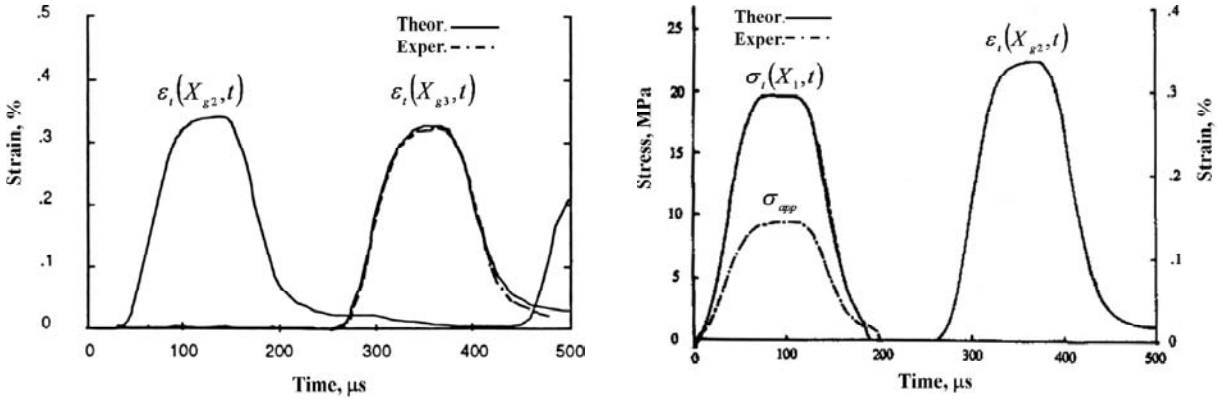

Fig 12. (a) The comparison between the dynamic strain $\varepsilon_t(X_{g3},t)$ measured and the prediction calculated from the measured $\varepsilon_t(X_{g2},t)$; (b) The comparison between the interface stress $\varepsilon_t(X_1,t)$ measured and the prediction calculated from the measured $\varepsilon_t(X_{g2},t)$.

if the transmitted stress wave in transmitted bar is calculated via multiplying the measured $\varepsilon_t(x_{g2},t)$ by an apparent elastic modulus E_a, namely $\sigma_{app}=E_a\varepsilon_t(x_{g2},t)$, which is also shown in Fig. 12b as labeled, then it can be found that, comparing with the actual transmitted stress $\sigma_t(X_1,t)$ on the interface, the error is as large as 52%.

5. RATE-DEPENDENT PROCESS OF DYNAMIC FAILURE

With regard to failure, the traditional method in a static failure analysis is: for a given material, of which a certain critical parameter such as strength, fracture toughness and crack opening displacement *etc*. has been determined from experiments, if any calculated mechanical value for a structure reaches or excesses this material parameter, then failure happens. However, material failure is essentially a time/rate-dependent process, which can be disregarded only when the duration of failure process, relative to the static loading duration, is negligible. In fact, if we use an intrinsic characterized time T_F to characterize the dynamic failure of material and use another characterized time T_L to characterize the duration of dynamic loading, when the T_L is as short as the same order of the T_F, then on one hand the time/rate-dependent process of material failure must be taken into account, including the evolution process of damage in all basic forms (such as voids, micro-cracks, localized shear bands *etc*.). On other hand, because of the propagation of failure zone (failure wave), the propagation of secondary stress waves induced by energy release due to failure, and their interactions with the stress waves originated by applied loading, the failure course will vary and become very complicated. Thus, the time/rate dependent dynamic failure of structures is inevitably in close relation with the time/rate dependent failure character of materials.

The following three most significant aspects of dynamic failure of materials under stress wave loading were studied by us and new models are proposed respectively.

5.1. Spalling model based on stress relaxation in the micro-damage coalescence process

According to the basic form of damage, spall can be classified as ductile spall and brittle spall.

In view of the fact that although mean void growth-based ductile spall models are successful for ductile spall, we have explored the possibility of presenting an equivalent mean crack growth-based failure model for brittle spall, and indicated that it remains to be demonstrated how an appropriate mean crack size is chosen to identify the brittle spall strength as the threshold pressure for crack growth. There seems to be no basis for a mean crack growth-based spall model which avoids nucleation considerations.

In fact, the threshold pressure P_g for the mean crack growth is [44]

$$p_g \approx \frac{K_{IC}}{\sqrt{R_m}}, \tag{5.1}$$

where K_{1c} is the fracture toughness, $R_m(\Omega)$ the shape parameter characterizing the crack distribution, called the mean crack size, and Ω the solid angle characterizing the crack orientation. Experiments suggest that the number of cracks per unit volume and orientation with a size greater than R remains approximately exponential during the deformation

process [44]. For an exponential distribution, the number density of cracks with a radius larger than R is given by

$$N(R,\Omega) = \int_R^{\infty} n(R,\Omega)\,\mathrm{d}R = N_0(\Omega)\exp\left(-\frac{R}{R_m(\Omega)}\right), \tag{5.2}$$

where $n(R,\Omega)$ is the number of cracks per unit volume, size and orientation with a crack radius in the range from R to $R + \mathrm{d}R$ and an orientation within the solid angle from R to $R + \mathrm{d}R$, $N_0(\Omega)$ the total number of cracks per unit volume.

The value of P_g estimated by Eq. (5.1) is much higher than the expected value. Thus, a new model for brittle spall is required considering the damage evolution during the brittle spall. We developed a crack straining-based spall model [45], assuming that the inelastic volumetric strain caused by the relaxed tensile pressure at a critical fragment volume is the main factor governing the solidity evolution in the process of coalescence and fragmentation, as follows.

(1) Express the solidity evolution in terms of inelastic volumetric strain rate

The solidity w is defined as:

$$w = V_s / \overline{V}, \tag{5.3}$$

where $\overline{V}$ is the total overall specific volume and V_s is the specific volume of the solid. Differentiation of Eq. (5-3) gives the volumetric strain rate:

$$\dot{\varepsilon}_{kk} = \frac{\dot{\overline{V}}}{\overline{V}} = \frac{\dot{V}_s}{V_s} - \frac{\dot{w}}{w}. \tag{5.4}$$

It is assumed that the total volumetric strain rate is composed of two parts: the elastic component $\dot{\varepsilon}^e_{kk}$ and the inelastic component induced by crack evolution (nucleation, growth and coalescence of cracks) $\dot{\varepsilon}^c_{kk}$, namely $\dot{\varepsilon}_{kk} = \dot{\varepsilon}^e_{kk} + \dot{\varepsilon}^c_{kk}$. It is further assumed that the elastic changes in w are small in comparison to the inelastic effects due to crack evolution. That is, the elastic volume change takes place at constant w. Therefore,

$$\frac{\dot{V}_s}{V_s} = \dot{\varepsilon}^e_{kk}, \tag{5.5}$$

$$\frac{\dot{w}}{w} = -\dot{\varepsilon}^c_{kk}. \tag{5.6}$$

(2) Determine the inelastic volumetric strain according to the crack opening strain and the crack shear strain.

The inelastic volumetric strain $\dot{\varepsilon}^c_{kk}$ per unit volume including crack opening strain and shear strain was given by Addessio and Johnson as [46]

$$\varepsilon^c_{kk} = 15\left(2-\nu\right)p\beta R_m^3, \tag{5.7}$$

where

$$\beta = \frac{64\pi}{15}\left(\frac{1-\nu}{2-\nu}\right)\frac{N_0}{G},$$

p is the pressure, ν and G are Poisson's ratio and shear modulus, respectively. It can be indicated that the average inelastic strain for a volume containing a system of cracks under tension is much larger than the volumetric strain due to the total elastic opening of the cracks [45]. Thus the evolution equation of solidity is obtained

$$\frac{\dot{w}}{w} = -\frac{128\pi\left(1-\nu^2\right)}{E}\frac{\mathrm{d}}{\mathrm{d}t}\left(pN_0R_m^3\right). \tag{5.8}$$

(3) Consider a crack straining-based spall model exploring the coalescence of cracks.

Coalescence occurs when the cracks become so large that they begin to intersect with other cracks. The relative volume of all the fragments in a distribution, τ_f, is given by Curran and Seaman [44] as

$$\tau_f = T_f\beta_1\gamma_1^3\tau_z, \tag{5.9}$$

where $\tau_z = 6N_0R_m^3$, $T_f \approx 4\pi/3$, $\beta_1 = 1/3\sim1/4$, $\gamma_1 \approx 1$. Therefore, $N_0R_m^3$ is closely related to the fragment volume τ_f during the process of coalescence and fragmentation. A crack straining based spall model is presented assuming that after the tensile pressure reaches spall strength $\tilde{p}_f$ the further decrease of the solidity is mainly due to the inelastic volumetric strain caused by the relaxed tensile pressure at a critical fragment volume ($N_0R_m^3$) during the process of coalescence and fragmentation. That is,

$$\mathrm{d}w = -\frac{128\pi\left(1-\nu^2\right)}{E}w\left(N_0R_m^3\right)_c\,\mathrm{d}\overline{p}, \tag{5.10}$$

where $\overline{p}$ is the averaged pressure in the composite of solid and cracks. When the solidity w reaches a critical value w_c the spa11 is supposed to become complete.

The model presented above was used to calculate the free surface velocity in the numerical simulation of the plane impact of plates and the results were compared with corresponding experimental data [47,48], as shown in Fig.13. The model reproduces free surface velocity fairly well, implying that the spallation information has been well captured.

We have applied the similar ideas to the spallation of ductile materials as well as the high-pressure constitutive relationship taking account of damage evolution, and the obtained results again agree well with experimental observations [49-51].

5.2. Brittle fragmentation model based on crack nucleation, growth, and interactions

This research starts from the work of numerical simulations, where we developed a Weibull strength theory based cohesive element, and applied this technique successfully to study the dynamic fractures and fragmentations of materials under impact loading [52-56]. Fig. 14 is an example showing a ceramic disk breaks into many pieces under centrifugal forces [56]. On this research basis, we will establish a more idealized model, and use the stress wave analytical approach to investigate the dynamic fragmentation process of brittle materials, including fragment size distributions, effects of material defects, relationship between failure strength and strain rate, *etc.* [57].

Under impact loadings, the failure of materials generally accompanies creations of many small pieces (fragments). An important issue to study the fragmentation process is to estimate the size of the fragments. The commonly used models to calculate fragment size is the Grady theory based on energy balance [58], and the Mott-Grady model based on statistical fracture [59,60]. Based on the assumption that the local kinetic energy is responsible for creating fractures within an expanding material, Grady provided a formula to calculate the average fragment size s:

$$S_{Grady} = \left(\frac{24 G_c}{\rho \dot{\varepsilon}^2} \right)^{1/3}, \tag{5.11}$$

where G_c is the fracture energy of the material, ρ the density, and $\dot{\varepsilon}$ the expanding strain rate. After taking account of the strain energy of a material before failure, Glenn and Chudnovsky revised the Grady formula as the following form [61]:

$$s_{G\&C} = 4\sqrt{\frac{\alpha}{3}} \sinh\left(\frac{\phi}{3}\right), \quad \phi = \sinh^{-1}\left[\beta\left(\frac{3}{\alpha}\right)^{3/2}\right],$$
$$\alpha = \frac{3\sigma_c^2}{\rho E \dot{\varepsilon}^2}, \quad \beta = \frac{3}{2}\frac{G_c}{\rho \dot{\varepsilon}^2}. \tag{5.12}$$

There are, however, sustained controversies over the assumption of the "local kinetic energy balance". Some recent theoretical and experimental work has shown that the classical energy balance theory significantly over-estimates the fragment sizes.

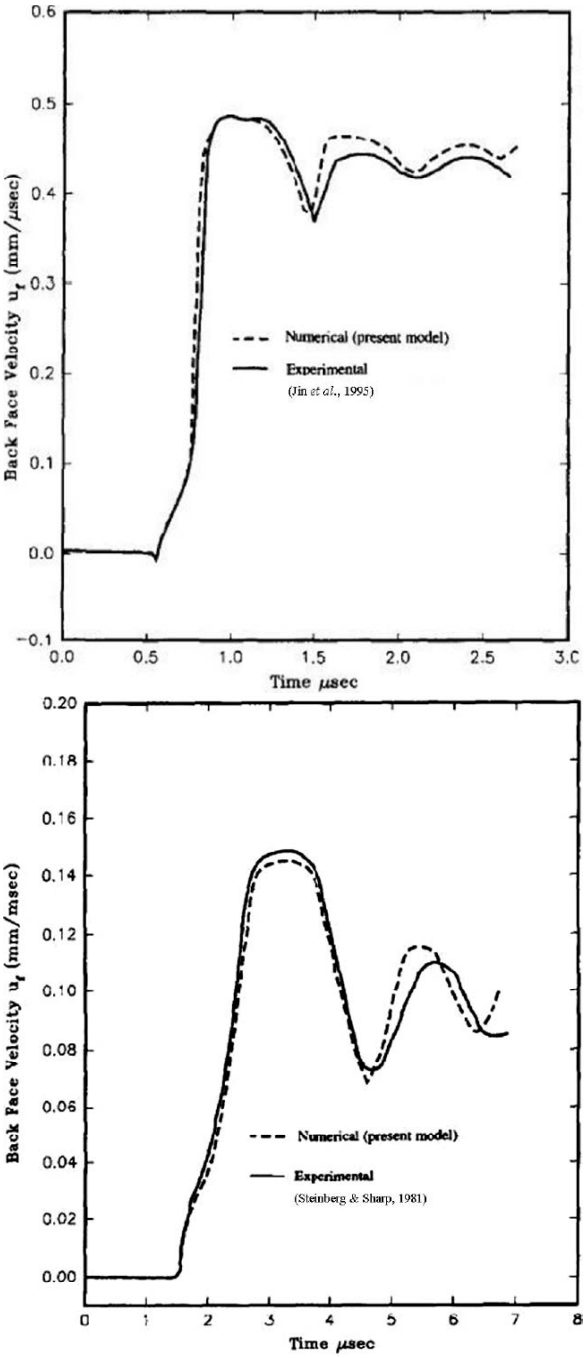

Fig. 13. Comparison of back face velocity history between experiment and calculation for: (a) ARMCO iron [47] and (b) uranium alloy [48].

We established a theoretical model to analyze the opening of a crack under stress wave loading and the interactions between cracks. For any crack that starts opening under critical stress σ_c, there is always an intrinsic length scale signifying fracture from initiation to complete failure (the so-called length of cohesive zone, which comes from the

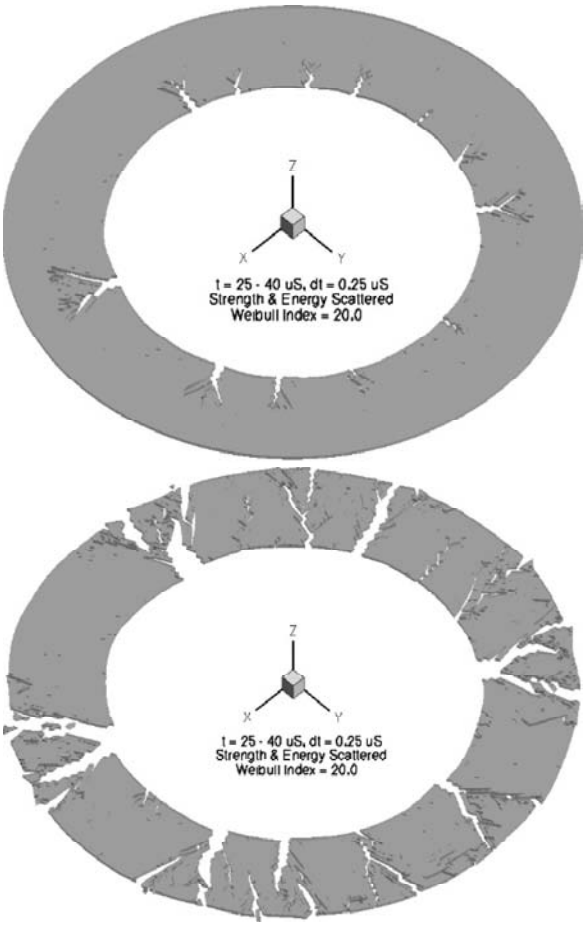

Fig. 14. The bursting (fragmentation) of a rapidly rotating disk under centrifugal force: (a) at the time $t = 8.43$ μs, showing the evolution of cracks, and (b) at the time $t = 25.4$ μs, the disk breaks into many pieces.

original concept of Dugdale [62] and Barenblatt [63]). An intrinsic time scale therefore exists that is controlled by the rapid unloading stress waves emitted from the opening crack. According to the compatible condition along the characteristic line, the cohesive fracture stress σ_{coh} and the cohesive crack opening velocity ν_{coh} satisfy the following dynamic condition:

$$\sigma_{coh}(t) - \sigma(X,0) = -\rho c\left[\nu_{coh}(t) - \nu(X,0)\right].$$

Assuming a linear decreasing cohesive law:

$$\sigma_{coh} / \sigma_c = 1 - \delta_{coh} / \delta_c,$$

where $\delta_c = 2G_c/\sigma_c$ is the critical crack opening distance at complete failure, $d\delta_{coh}/dt = \nu_{coh}$. Solving the above ODEs with the initial condition $t = 0{:}\delta_{coh} = 0$, $\sigma_{coh} = \sigma_c$ gives rise to the solution $\delta_{coh}(t)$, and subsequently the critical time t_f at which fracture is completed ($\delta_{coh}(t_f) = \delta_c$),

$$\left(\frac{\dot{\varepsilon}}{C_0\sigma_c^3 / E^2 G_c}\right)\left\{\exp\left[\frac{C_0 t_f}{EG_c / \sigma_c^2}\right] - \frac{C_0 t_f}{EG_c / \sigma_c^2} - 1\right\} = 1, \tag{5.13}$$

where $C_0 = \sqrt{E/\rho}$ is the elastic wave velocity. As the opening crack unloads the neighboring zone, the total length of unloading zone $C_0 t_f$, considered as the fragment size under the concept of Dynamics of Isolated Decohesion (DID), is expressed implicitly in Eq. (5.13).

Consider now the characteristic scales in a fragmentation process. We see that there exist a characteristic strain rate $\dot{\varepsilon}_0$ and a characteristic fragment size s_0, determined exclusively by the material parameters E, C_0, G_c, and σ_c:

$$\dot{\varepsilon}_0 = C_0\sigma_c^3 / E^2 G_c, \quad s_0 = EG_c / \sigma_c^2. \tag{5.14}$$

Introducing the nondimensional strain rate and nondimensional fragment size defined as

$$\bar{s} = s / s_0, \quad \bar{\dot{\varepsilon}} = \dot{\varepsilon} / \dot{\varepsilon}_0, \tag{5.15}$$

the formulae of Grady and Glenn-Chudnovsky can be simplified, respectively, as:

$$\bar{s}_{Grady} = \left[\frac{24}{(\bar{\dot{\varepsilon}})^2}\right]^{1/3}, \tag{5.16}$$

$$\bar{s}_{G\&C} = \frac{4}{\bar{\dot{\varepsilon}}}\sinh\left[\frac{1}{3}\sinh^{-1}\left(\frac{3}{2}\bar{\dot{\varepsilon}}\right)\right], \tag{5.17}$$

while the nondimensional fragment size based on DID theory is expressed implicitly as:

$$\exp\left(\bar{s}_{DID}\right) - \bar{s}_{DID} - 1 = \bar{\dot{\varepsilon}}^{-1}. \tag{5.18}$$

It is seen that either for the energy models or for the DID model, the nondimensional fragment size is only determined by the nondimensional strain rate.

In fact, in a realistic fragmentation process, multiple cracks can be nucleated as the material is expanding. A part of the nucleated cracks, however, will stop growing due to the unloading effects between the cracks. To investigate the full interaction process, we extend the previous analytic approach to the numerical approach with complex wave calculations. In a numerical simulation, the nucleation of cracks are random in space. The growth behaviors of the nucleated cracks are again described by the linear cohesive law. Under a prescribed extending rate (strain rate), the complete fragmentation process is full simulated by

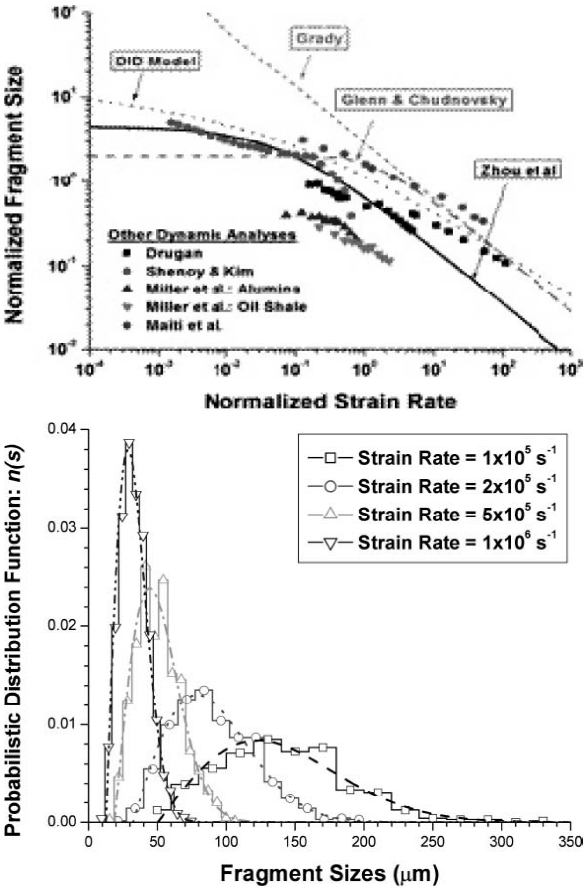

Fig. 15. Fragment size and fragment size distribution: (a) the nondimensional "fragment size vs. strain rate" relationships of different models, and comparisons with discrete numerical data; (b) the character of fragment size distribution at different strain rate.

incorporating the cohesive fracture law with the method of characteristics. Each simulation gives the total number of the fragments and the size of each fragment. We have simulated the fragmentation process of 11 materials under different strain rates, obtaining the curves of "average fragment size *s* verse strain rate $\dot{\varepsilon}$". These curves are different for different materials, however, they collapse into a master one after *s* and $\dot{\varepsilon}$ are normalized by the corresponding characteristic scales s_0 and $\dot{\varepsilon}_0$. The nondimensional $\dot{\sigma}$-$\bar{\dot{\varepsilon}}$ curve is shown in Fig. 15a, which can be fitted by the following empirical formula:

$$\bar{s}_{ZMR} = \frac{4.5}{1+6.0\bar{\dot{\varepsilon}}^{2/3}}. \qquad (5.19)$$

Comparing the four curves predicted by Eqs. (5.16) to (5-19), respectively, as plotted in Fig.15, it is seen that in the quasi-static region ($\bar{\dot{\varepsilon}}$<<1), our model (Eq. (5.19) gives fragment size 4.5, which is more than twice the value 2.0 provided by Glenn and Chudnovsky. The reason is that in a brittle fragmentation process, once the cracks are nucleated the rapid unloading of the material induces stress wave propagation, which consumes about half of the stored strain energy. The remaining strain energy is transferred to the fracture energy, creating fragments half the number of the Glenn-Chudnovsky's estimation. To the other end, namely in the dynamic region ($\bar{\dot{\varepsilon}}$>>1), our curve is parallel to the lines of energy models (Eqs. (5.16) and (5.17)), implying that these models have the same scaling property. Nevertheless, the absolute value of our calculated fragment size is about 1/4~1/5 of the Grady model. This means that the classical "local kinetic energy assumption", which is the basis of the Grady formula (and Glenn-Chudnovsky formula, too), is not correct for a realistic fragmentation process. In fact, no matter how rapid a fragmentation could be, it is always a time-dependent process during which the material system can extract much more energy from the initial translational energy than the "local kinetic energy" conjectured by Grady. This energy is transferred into the fracture energy, creating much more, much small fragments. In Fig. 15a we also compared our results with those obtained by other researchers, it is seen that our curve (Eq. (5.19) is close to the average of the discrete data obtained in other dynamic models based on stress wave propagation. We have also compared our results with the available experimental data, and found that our curve is reasonably close to them. Moreover, from the average fragment size, the character of fragment size distribution can be further calculated, as typically shown in Fig. 15b.

5.3. Adiabatic shearing failure

Adiabatic shearing failure due to the evolution of adiabatic shear band is one of the most distinguished forms of dynamic failure under explosive/impact loading, which widely exists in the processes of high-speed deformation, penetration, plugging, high-speed formation, cutting, erosion, *etc.*

Adiabatic shearing phenomenon is usually characterized by two basic facts which are corresponding to each other: macroscopically, the so-called apparent constitutive instability is experimentally observed, namely, the apparent stress-strain curve of the material changes from strain hardening ($d\sigma/d\varepsilon > 0$) to strain softening ($d\sigma/d\varepsilon < 0$); and microscopically, the so-called highly localized shear band is experimentally observed, which is such a local region that either shear deformation is intensively

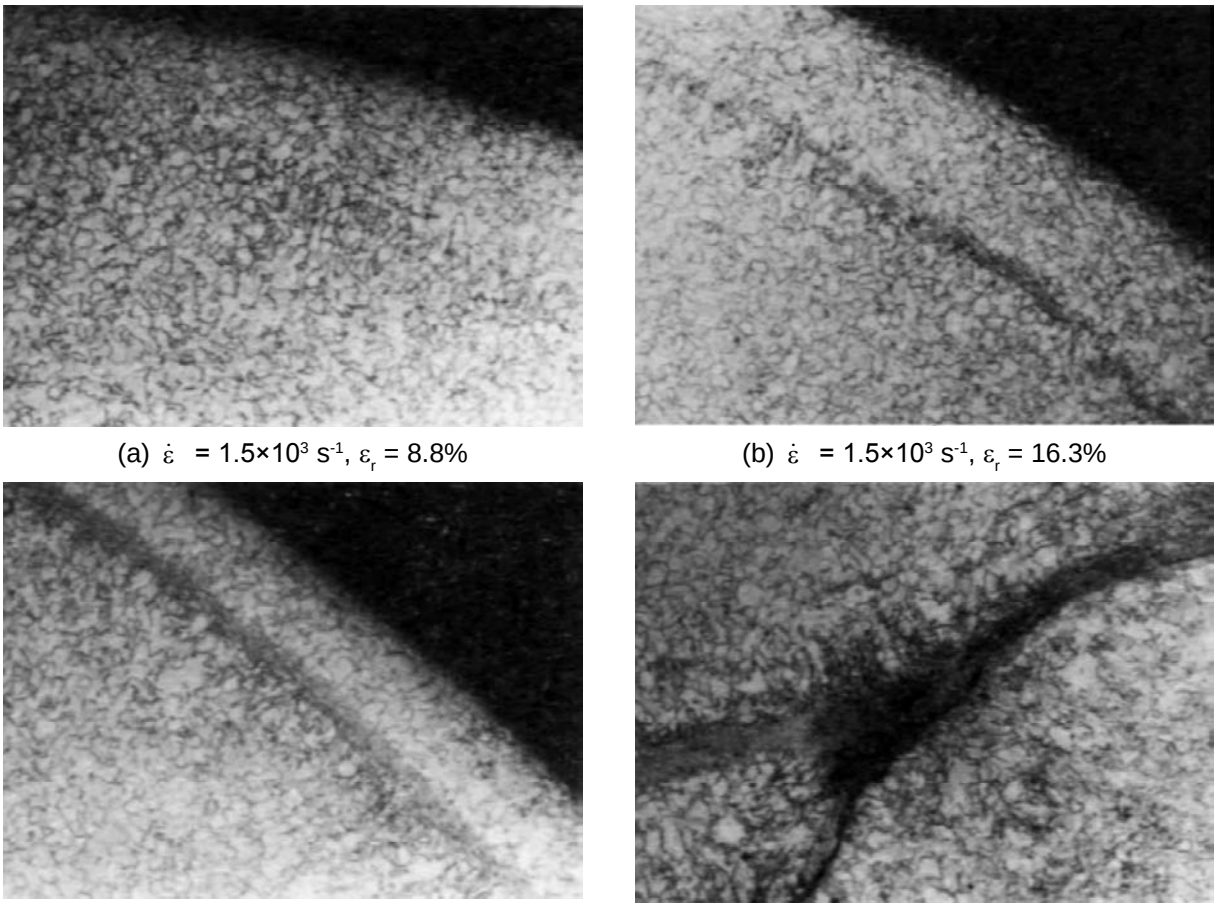

(a) $\dot{\varepsilon}$ = 1.5×10^3 s^{-1}, ε_r = 8.8%

(b) $\dot{\varepsilon}$ = 1.5×10^3 s^{-1}, ε_r = 16.3%

(c) $\dot{\varepsilon}$ = 1.5×10^3 s^{-1}, ε_r = 27.4%

(d) $\dot{\varepsilon}$ = 1.5×10^3 s^{-1}, ε_r = 42.3%

Fig. 16. Micrographs (100X) of TB2 specimens after impact tests, showing the development of adiabatic shear band with the increase of strain for a given strain rate 1.5x10^3 s^{-1}.

localized without micro-structure change (called deformed shear band) or the material within the band has undergone a transformation of micro-structure (called transformed shear band).

5.3.1. Thermo-viscoplastic constitutive instability

Zener and Hollomon [64] firstly attributed the adiabatic shearing to the balance/competition between the strain hardening mechanism and the thermal softening mechanism due to heat converted from plastic dissipation. When the effect of thermal softening exceeds the effect of hardening, apparent constitutive instability occurs, called thermo-plastic instability.

Since then, various criteria for the adiabatic shearing have been established, including critical strain-rate criterion by Recht [65] and the critical strain criterion by Culver [66], *etc.*, all are one-control-variable criteria. However, there is no criterion which takes both strain and strain-rate effect into consideration, needless to say the temperature, although the adiabatic shearing phenomenon usually occurs under high strain rates and at finite deformation, and particularly in low temperature. We for the first time proposed a model of thermo-viscoplastic instability, taking into account of effects of strain, strain rate and temperature [67,68]. In fact, from a series of macro-/microscopically combined experimental investigations on the adiabatic shear process for a β-titanium alloy TB2 (Ti-8Cr-5Ni-5V-3Al) and Ti6Al4V, it is revealed that adiabatic shear of material is not a suddenly happening event but a rate-dependent and temperate-dependent processes, including the nucleation and growth of the deformation band, the transition from the deformed band to the phase-transformed band, the development of phase-transformation band, crack initiation and extension along the shear band, until the final failure [68-72]. Typical micro-observations are given in Figs. 16 and 17. As can be seen from those figures, adiabatic shear bending is markedly dependent on both strain and strain rate.

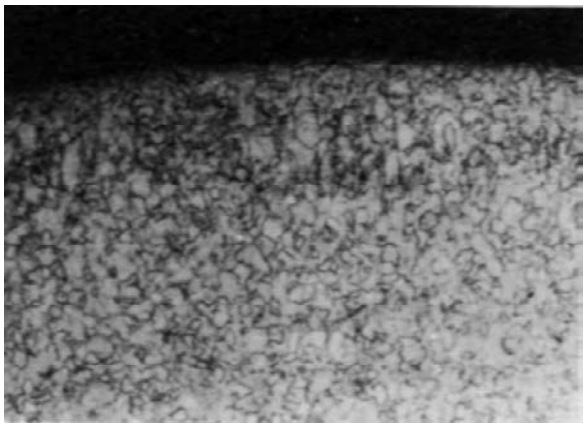

(a) $\dot{\varepsilon}$ = 0.88×10^3 s^{-1}.

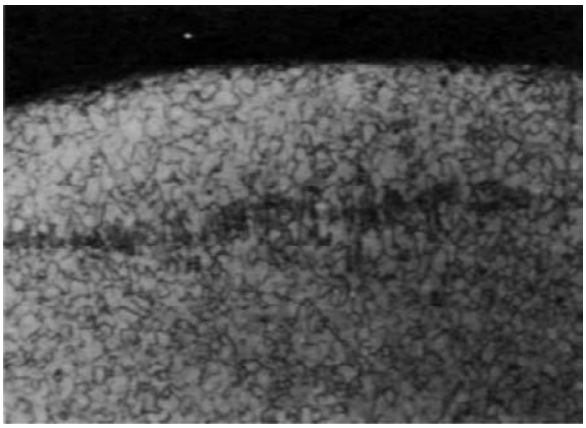

(b) $\dot{\varepsilon}$ = 1.45×10^3 s^{-1}.

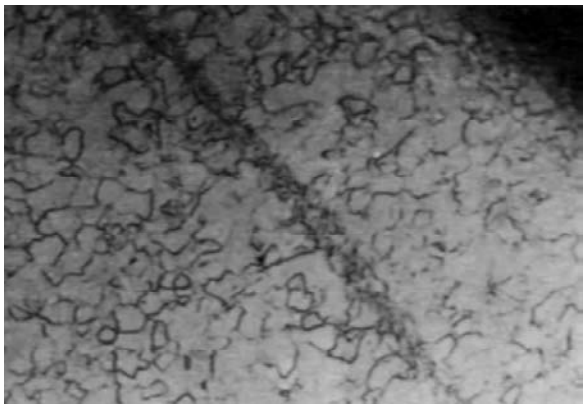

(c) $\dot{\varepsilon}$ = 2.21×10^3 s^{-1}.

Fig. 17. Micrographs of TB2 specimens after impact tests, showing the development of adiabatic shear band with the increase of strain rate for a given strain 16%.

Theoretically, taking account of the important role played by the strain rate, an adiabatic shearing criterion based on the concept of thermo-viscoplastic instability can be established as follows.

Assume a general form of thermo-viscoplastic constitutive equation:

$$\tau = f(\gamma, \dot{\gamma}, T), \tag{5.20}$$

where τ denotes the shear stress, γ the shear strain, $\dot{\gamma}$ the shear strain-rate and T the temperature. Obviously, the corresponding critical condition for constitutive instability is

$$\frac{\mathrm{d}\tau}{\mathrm{d}\gamma} = \frac{\partial\tau}{\partial\gamma} + \frac{\partial\tau}{\partial\dot{\gamma}}\frac{\mathrm{d}\dot{\gamma}}{\partial\gamma} + \frac{\partial\tau}{\partial T}\frac{\mathrm{d}T}{\partial\gamma} = 0, \tag{5.21}$$

where $\partial\tau/\partial\gamma$ denotes the strain-hardening, $\partial\tau/\partial\dot{\gamma}$ the strain-rate hardening and $\partial\tau/\partial T$ the thermo-softening. Under adiabatic condition, we have the well-known relation connected the adiabatic temperature-rise dT and the visco-plastic deformation work τdγ

$$\mathrm{d}T = \frac{\beta\tau\,\mathrm{d}\gamma}{\rho c}, \tag{5.22}$$

where ρ the density of material, C the specific heat, and β the Taylor-Quinney coefficient describing the fraction of viscoplastic work converted to heat. In principle, T can be solved from Eq. (5.22) as a function of γ and $\dot{\gamma}$, and consequently the critical condition (Eq. 5.21) can be regarded as a first order ordinary differential equation of $\dot{\gamma}$ with respect to γ. It means that, unlike Recht's, Culver's and others one-control-variable criterion, the critical condition for adiabatic shear instability $f_c(\gamma, \dot{\gamma}) = 0$ now contains two control-variables, $\dot{\gamma}$ and γ, which is corresponding to a set of $\dot{\gamma}$ - γ curves,.

If the thermo-viscoplastic constitutive equation (Eq. 5-21) is realized in the form of

$$\tau = \tau_0\gamma^n\left(1 + g\ln\frac{\dot{\gamma}}{\dot{\gamma}_0}\right)\left(1 - \alpha\frac{T}{T_0}\right), \tag{5.23}$$

then the corresponding critical condition for adiabatic shearing can be expressed as

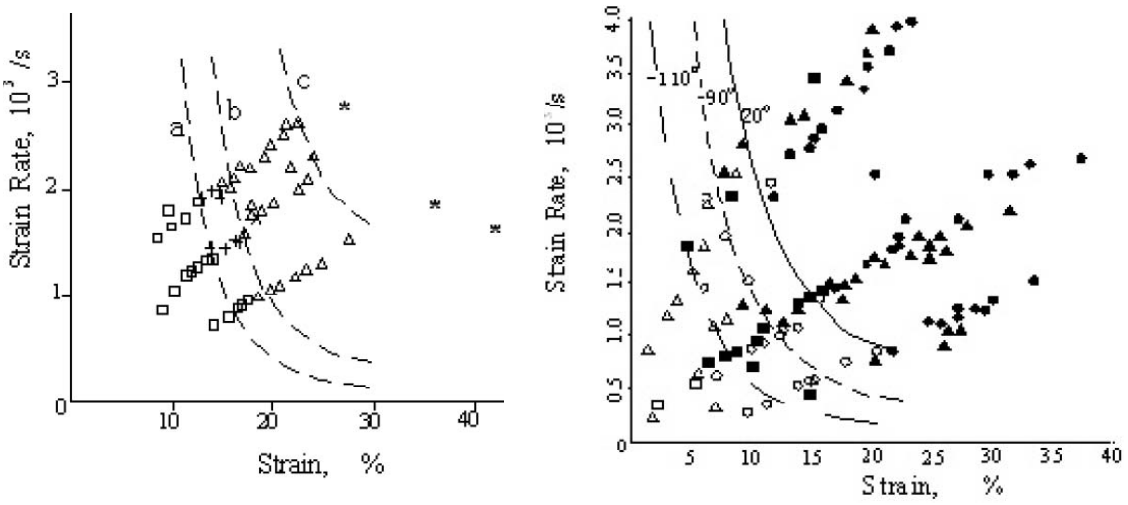

Fig. 18. Dependence of the adiabatic shear band evolution and fracture for titanium alloy on the strain, strain-rate and temperature: (a) Experimental results for TB2 under room temperature, □ - without shear band, + - deformation band, Δ - phase-transformation band, * - fracture; theoretical curves a, b, and c corresponding to A=1.1536, 1.1382, and 1.1143, respectively. (b) Experimental results under different temperature, O - 20 °C, D - 90 °C, □ - 110 °C; hollow symbol—without shear band, solid symbol—with shear band; A(-90 °C)=0.8918 and A(-110 °C)=0.9028.

$$\left(1+g\ln\frac{\dot{\gamma}}{\dot{\gamma}_0}\right)\left(A-\frac{\alpha\beta\tau_0}{T_0\rho c}\gamma\right)\gamma^n=1, \qquad (5.24)$$

where n, g and α are material parameters characterizing strain hardening, strain-rate hardening and thermal softening respectively, τ_0, $\dot{\gamma}_0$, and T_0 are the characteristic stress, strain rate, and temperature, respectively, and A is an integral constant characterizing a certain state in the adiabatic shearing process, such as the initiation of shear band, the transformation of micro-structure of shear band, the arrival of a certain temperature, *etc*. Sets of adiabatic shearing critical conditions for other forms of thermo-visoplastic constitutive equations are also derived [67,71,72]. Furthermore, regarding the parameter A as a function of test temperature (environmental temperature) T_e, $A(T_e)$, the critical condition for adiabatic shear instability $f_c(\gamma,\dot{\gamma})=0$ can be generalized to take environmental temperature into account, $f_c(\gamma,\dot{\gamma},T_e)=0$. It means that the critical condition for adiabatic shearing evolution should be a tri-variables criterion with three controlled variables: strain-rate, strain and temperature [68,71]. Results of SHPB experiments for titanium alloys TB2 and Ti6Al4V have shown that the theoretical predictions agree with the experimental results very well. Typical results for TB2 are shown in Fig. 18a under room temperature and (b) under low temperatures, respectively.

Since adiabatic shearing is a strain-localization phenomenon, similar to a micro-mechanics approach, a numerical analysis of strain-localization for the material with defective region (weak region) was developed by us to analyze the adiabatic shearing process [73]. For the β-titanium alloy TB2, which is strongly susceptive of adiabatic shearing, the numerical simulation reveals that for a given average high strain rate (e.g. 10^3 s^{-1}), there exist three phases in a high velocity deformation process. In the early phase, the strain-hardening plays a dominant role, showing a tendency of strain-homogenization. However, with increase of average strain, the thermal softening begins to play a dominant role and consequently a transition from a strain-homogenization process to a strain localization process appears. Finally the accelerated strain-localization process leads to a dramatically increase of the strain and temperature in the localized region, which is corresponding to the adiabatic shearing or thermo-viscoplastic instability. Thus the same conclusion as that found from the experimental observations and theoretical analysis is obtained, namely the critical condition for adiabatic shearing is controlled by strain, strain rate and temperature.

5.3.2. Interaction between crack and adiabatic shearing

It is of basic significance to study the interaction between crack and adiabatic shearing, which should be studied from a knowledge combining both adiabatic shearing criterion and fracture mechanics.

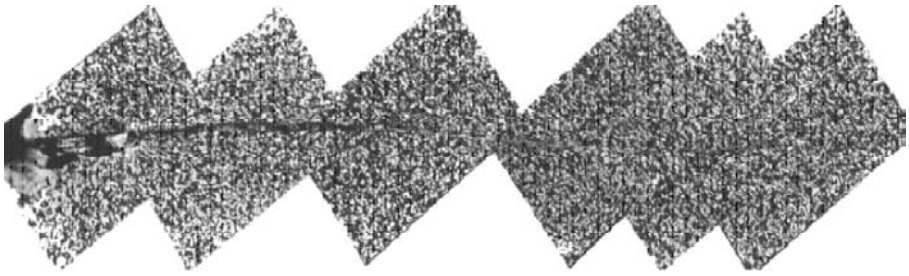

Fig. 19. Typical micrograph of a mode-II crack extending along the precursory adiabatic shear band.

Kalthoff [74,75] firstly reported that for a dynamic Mode-II crack, two failure modes exist. At low loading rates, the usual failure mode predominated by e.g. the maximum tensile stress criterion was observed, i.e. cracks propagate at an angle of about 70° with respect to the ligament; while when the loading rate exceeds a certain limit, an adiabatic shearing failure mode predominated by the localized shear banding was observed and the cracks propagate along their original direction.

Using Hopkinson Pressure Bar technique, we investigated quantitatively the condition of adiabatic shear fracture of Mode-II crack for titanium alloy Ti-6Al-4V. From microscopic observation, it was found that the adiabatic shear extension of mode-II crack basically consists of three stages in succession. Firstly, promoted by the highly concentrated dynamic stress/strain/strain-rate field in front of the crack tip, a highly localized shear band develops ahead of the crack along the original crack direction. Then, voids appear and grow within the shear band, particularly ahead of the crack tip. Finally, the crack propagates along the shear band by a mechanism of voids coalescence. A typical microstructure of adiabatic shearing failure of mode-II crack is shown in Fig. 19.

Starting from an analysis combining both the critical condition of thermo-viscoplastic instability for adiabatic shearing and the stress/strain field of a Mode-II crack, a thermo-viscoplastic instability criterion, with two-control variables in terms of the stress intensity factor K_{II} and its rate $\dot{K}_{II}$, for the adiabatic shearing initiation of a dynamic mode-II crack was proposed [76].

For titanium alloy Ti-6Al-4V, our experiments show that its thermo-viscoplastic constitutive equation can be described by the following equation

$$\sigma = \left(\sigma_0 + E_1\varepsilon\right)\left(1 + g\ln\frac{\dot{\varepsilon}}{\dot{\varepsilon}_0}\right)\left(1 - \alpha\frac{T}{T_e}\right). \qquad (5.25)$$

Similar to Eq. (5.24), the corresponding critical condition for adiabatic shearing is

$$\left(\frac{\sigma_0}{E_1} + \varepsilon\right)\left(1 + g\ln\frac{\dot{\varepsilon}}{\dot{\varepsilon}_0}\right)\left[A(T_e) - \frac{\alpha\beta E_1}{\rho C_v T_e}\right] = 1. \qquad (5.26)$$

Then the adiabatic shearing initiation of a dynamic mode-II crack is finally obtained as [77]:

$$\left(1 + g\ln\frac{2(1+\nu)K_{II}\dot{K}_{II}}{\pi E\sigma_0\dot{\varepsilon}_0 r_c}\right)\left(\frac{\sigma_0}{E_1} + \frac{(1-\nu)K_{II}^2}{\pi E\sigma_0 r_c}\right)\times \left(A - \frac{\alpha\beta E_1}{\rho C_v T_e}\frac{(1+\nu)K_{II}^2}{\pi E\sigma_0 r_c}\right) = 1, \qquad (5.27)$$

where E is Young's modulus, ν the Poisson's ratio, A and r_c are material parameters. For the Ti-6Al-4V tested, it was experimentally found that $r_c = 0.8$ μm and $A = 0.86$. Obviously, Eq. (5.27) is a generalization of Eq. (5.26) for materials without crack to the case of materials with Mode-II cracks.

The theoretical predictions given by Eq. (5.27) are supported by the experimental results, as shown in Fig. 20.

6. ENGINEERING APPLICATIONS OF STRESS WAVE THEORIES

Creative contributions to engineering application were made by us, based on the mentioned studies on the theories of stress wave and dynamic mechanical properties of materials and structures. Three typical applications are described below.

6.1. Impact dynamics study on security of an aircraft undergoing bird-impact

Base on experimental research on impact behavior of aviation materials and the theory of stress wave, the dynamic responses of aircraft windshields and wings to bird-strike were investigated from the viewpoint of impact dynamics [38]. The experimental results of a windshield PMMA tested at the strain-rates of 10^{-4} s^{-1} to 10^{3} s^{-1} and the temperatures of -

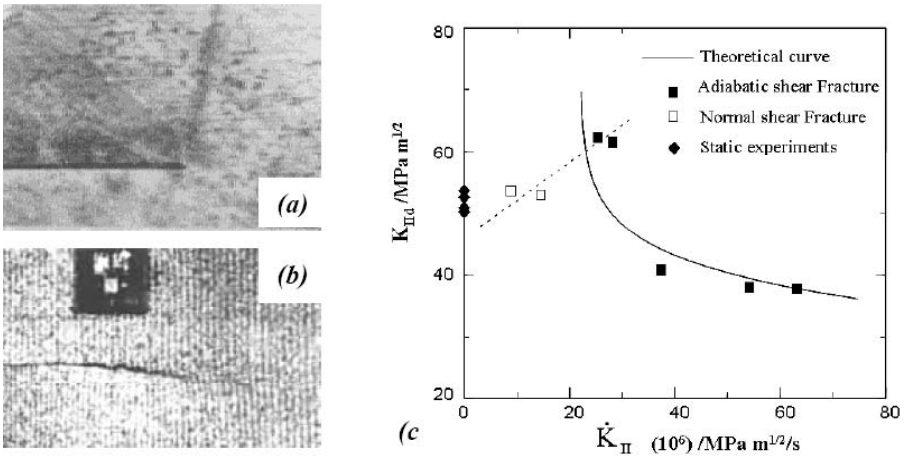

Fig. 20. Fracture patterns and the relationship between K_{IId} and $\dot{K}_{II}$ for mode-II crack initiation, (a) usual shear fracture, (b) adiabatic shear fracture, (c) comparison of theoretical predictions with experiments for the K_{IId} versus $\dot{K}_{II}$ relation.

Fig. 21. The prototype test of a aircraft wing struck by a bird, the bird weight is 1.8 kg and the impact velocity is 355 m/s, (a) before the impact and (b) after the impact.

60 to 100 °C were obtained (see e.g. Fig. 7), and a corresponding nonlinear thermo-viscoelastic constitutive equation was suggested [78]. The dynamic responses of a cast magnesium alloy under the strain-rates of 10^{-4} s^{-1} to 10^{3} s^{-1} were also determined, and a corresponding apparent nonlinear elasto-plastic constitutive equation was suggested, taking account of both the rate-dependent hardening effect and the damage-induced weakening effect [79]. The character of impact loading was also numerically analyzed. The agreement between the numerical predictions and experimental measurements are satisfactory enough.

Figs. 21a and 21b describe the prototype test of an aircraft wing struck by a bird, of which the weight is 1.8 kg and the velocity is 355 m/s. As can be seen, the deformation of wing is highly localized and instabilized.

It should be emphasized that the determination of impact loading is coupled with the dynamic response of structures, and the constitutive characters of both the bird and the windshields/wings markedly influence the total impact loading. These researches were performed to ensure the security of flight and to satisfy international trade requirements.

6.2. Improvement of split Hopkinson pressure bar technique by using visco-elastic bars

It has been widely accepted that material behavior at high strain rates can be studied experimentally by using split Hopkinson pressure bars (SHPB) [80]. However, SHPB is only an experimental facility to conduct high strain rate tests. For different engineering materials, the experimental data obtained should be further analyzed from the theory of stress wave propagation and the theory of material constitutive relationship, so that could be applied in numerical simulations and design analyses. According to requirements of different projects, dynamic responses under high strain rates of over one hundred engineering materials were studied by

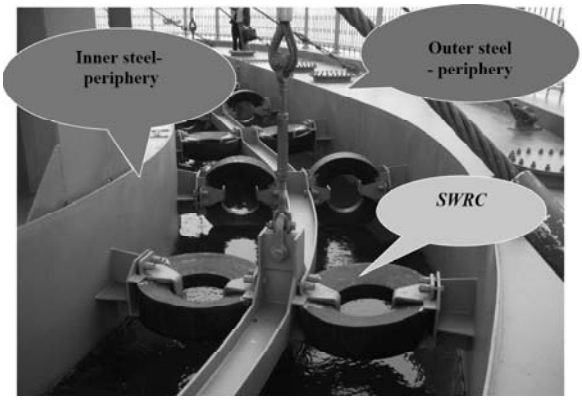

Fig. 22. An actual application of SWRC flexible crashworthy device.

us using SHPB together with other supplementary testing means. A lot of data depicting material behavior at strain rate 10^{-3}~10^{3} 1/s were obtained, and the corresponding constitutive models have been proposed. The proposed constitutive equations have been incorporated into commercial impact dynamics codes to analyze various engineering design, such as electronic components, communication instruments and packing structures, and so on [26-30,36-38].

The pressure bars in traditional SHPB are usually made of high strength steel with a high elastic limit σ_s >1 GPa and a corresponding wave impedance $(\rho_0 C_0)_{bar}$ of about 40 MPa s/m, while the elastic limit and wave impedance $(\rho_0 C_0)_{spec}$ of specimen are generally relative lower, so that the specimen could deform non-elastically while the bars still work within its elastic state during experiments. However, if the wave impedance $(\rho_0 C_0)_{spec}$ of specimen is much lower than that of bars, the signal of transmitted pulse will become too weak so that it could not be detected accurately. In such a case, it seems that a bar material with lower acoustic impedance should be used instead of a high strength steel.

In fact, for soft materials such as solid propellant of rockets, foams and biomaterials, the wave impedance $(\rho_0 C_0)_{spec}$ of specimen is as lower as in the order of 0.1 to1 MPa/m/s, so that the traditional SHPB with high strength steel bars is no longer suitable for testing those low impedance soft materials. Some researchers tried to replace steel bars by polymer (PMMA, nylon...) bars to reduce the wave impedance, but they still adopt the traditional assumptions of SHPB where the behavior of bar is elastic. As previously pointed out in the Sub-Section 4.3, there exist attenuation and dispersion of stress waves as they travel in visco-elastic bars [11]. The attenuation and dispersion produce errors in analyzing experimental data, which should be modified by considering the propagation of visco-elastic waves in polymer bars.

We, for the first time, dealt with this problem by using the theory of visco-elastic waves and obtain correct solutions [43,81]. This new technique was evaluated as one of the major developments in SHPB testing [82], and was successfully used to investigate the dynamic behavior of small-sized cellulose nitrate foil [83].

6.3. Creative design and analysis of a new flexible, energy-dissipating crashworthy device against ship-bridge collision

Following the computation based on the theory of stress wave and the theory of nonlinear visco-elastic constitutive modeling, a new flexible, energy-dissipating crashworthy device against ship-bridge collision has been built [84-86]. The highlights in designing this device are listed below.

6.3.1. A new design and analysis of the flexible, energy-dissipating crashworthy device

The collision between a ship and a bridge happens in very short time period, maybe several milliseconds or several seconds, during which intense energy exchange occurs. To design a protection device, it is needed to figure out collision forces. But, existing formulas in handbooks to calculate impact forces are semi-experiential ones, substantially based on simple models of collision between rigid bodies or elastic ones. These formulas are based on quasi-static analysis via energy conservation of an elastic

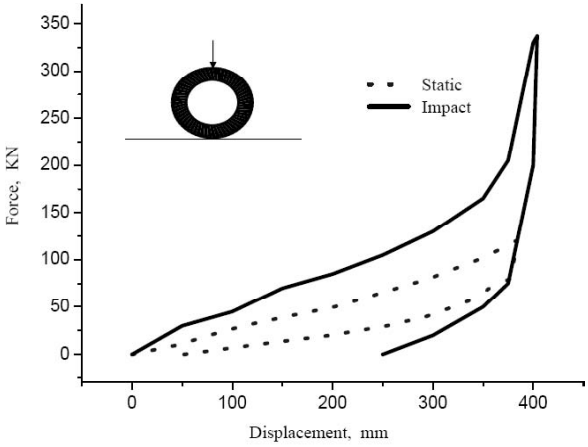

Fig. 23. The *F-u* curves of SWRC in quasi-static and impact loading.

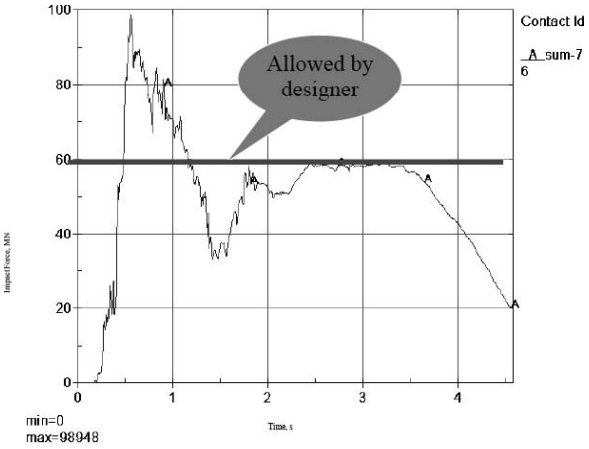

Fig. 24. Impact force $F(t)$ calculated when ship directly impacts onto bridge pier without protective device.

system, but characteristics of dynamics such as stress waves, strain rate effects of materials are not considered; nor intensive localization, local dynamic buckling of structures and dynamic fracture, etc. We presented that impact force should be determined by the coupling effects of stress waves between a ship and a bridge-pier (or a protection device). The propagation of stress waves varies obviously on different materials and structures, initial and boundary conditions. At this view, it is not possible to represent such a complicated dynamic phenomenon with a simplified quasi-static formula. Following the theory of stress wave and the theory of rate-dependent constitutive model, we presented special solutions to special problems.

6.3.2. Mechanics model of a steel-wire-rope coil (SWRC)

Basic components of the new flexible, energy-dissipating crashworthy device are steel-wire-rope coils (SWRC), which are connected in parallel and series and furthermore connected with inner and outer periphery of the device and floating around a pier (Fig. 22). Obviously, the key to simulate the device is properly modeling those SWRCs. Our experiments show that [85] the force-displacement curve of SWRC, *F-u*, on one hand displays a concave upward and a loading-unloading hysteresis loop, showing an initial low stiffness (or high flexible) and energy-dissipating response. On other hand it is dependent on strain rate, as shown in Fig. 23. Such *F-u* character, like of polymers, can be modeled by ZWT rate-dependent nonlinear viscoelastic body (c.f. Eq. (4.1), and described by Eq. (6.1).

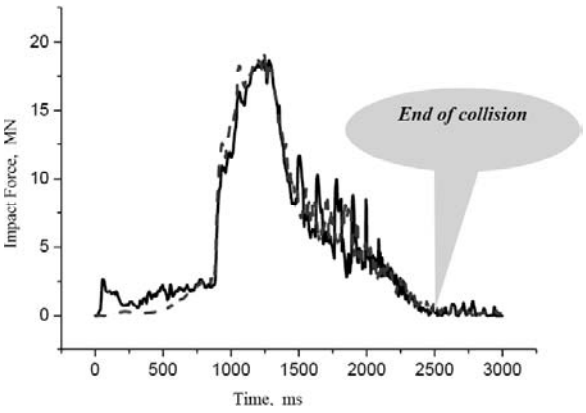

Fig. 25. Impact force $F(t)$ calculated: solid line - $F_O(t)$ at outer interface, dotted line - $F_I(t)$ at inner interface.

$$F = K(u)u + K_2 \int_0^t \nu(\tau) \exp\left(-\frac{t-\tau}{\theta_2}\right) \mathrm{d}\tau, \qquad K(u) = K_a + K_\alpha u + K_\beta u^2, \tag{6.1}$$

where F is the force (N), u the displacement (mm), ν the impact velocity (m/s), $K(u)u$ describes the nonlinear elastic equilibrium response, K_2 (N/mm), and θ_2 (ms) are the elastic coefficient and relaxation time at high strain rates, respectively. All parameters can be obtained through fitting experimental data.

6.3.3. Numerical simulation of the collision between a ship and a bridge-pier with a SWRC device

Dynamic numerical simulations are completed for full size ship-bridge collision when a ship with carrying capacity of 50,000 tons impacted onto a bridge-pier at the impact velocity of 4 m/s [84]. The numerical results show that, when the ship directly impacts onto the bridge pier, the impact force reaches 100 MN, much large than the critical value (60 MN) allowed by designers (Fig. 24), while when the SWRC flexible crashworthy device is installed, the impact force is greatly reduced, less than 20 MN (Fig. 25)!

As can be seen from Fig. 25, in the collision beginning up to about 800 ms, the impact force is quite low (only about 2.5 MN), an expected result due to the flexible character of SWRC. After roughly 800 ms, the $F_O(t)$ at outer interface and the $F_I(t)$ at inner interface approach equilibrium and sharply increase, indicating that the device now begins to work as a whole. At t=1.3 s, $F(t)$ reaches its maximum (18 MN) and then decreases. Comparing with the numerical animation, it corresponds to the

situation that the ship bow has changed its original course. At t = 2.5 s, $F(t)$ almost decreases to zero, indicating the end of collision.

Numerical simulations of different incidence collision angles were performed [86] and the results show that impact force, kinetic energy transported and deformation energy increase as the incidence angle decreases. However, the maximum impact forces are still smaller than the criterion allowed (60 MN), so that the design satisfies safety requirement.

Our study shows that SWRCs are suitable to be components of a new crashworthy device due to its flexible, energy dissipation and rate-dependence. The ZWT nonlinear viscoelastic model can be used to depict the dynamic behavior of SWRC for finite element simulations. The new device markedly reduces the impact force, and particularly enables the ship having enough time to turn its navigation direction under lower impact force. Consequently, the turning-away ship could carry a large percentage of initial kinetic energy of ship away. It is thus very conducive to the safety of both the bridge and the ship.

ACKNOWLEDGEMENT

Project supported by the National Natural Science Foundation of China (No.10872101, 11032001), as well as sponsored by K. C. Wong Magna Fund in Ningbo University.

REFERENCES

[1] T. von Karman, H.F. Bohnenblust and D.H. Hyers, The Propagation of Plastic Waves in Tension Specimens of Finite Length. Theory and Methods of Integration, *NDRC Report A-103(1942).*

[2] Kh. A. Rakhmatullin // Rus. Appl. Math. Mech. **9** (1945) 91, In Russian.

[3] E.H. Lee // *Quart. Appl. Math.* **10** (1952) 335.

[4] A.M. Skobeev // Rus. Appl. Math. Mech. **26** (1962) 1059, In Russian.

[5] R.J. Clifton and T.C.T. Ting // *J. Appl. Mech.* **35 (**1968) 812.

[6] T.C.T. Ting // *J. Appl. Mech.* **38** (1971) 441.

[7] J. Yu, L. Wang and Z. Zhu // *Kexue Tongbao* (*A Monthly Journal of Science*) **v.27** (1982) 574.

[8] J.-L. Yu, L. Wang and Ch.-H. Chu // *Acta Mechanica Solida Sinica* **3** (1982) 313, in Chinese.

[9] L. Wang, Ch.-H. Chu and J.-L. Yu // *Explosion and Shock Waves* **v.33,** No.1 (1983) 1.

[10] J.-L. Yu, L. Wang and Ch.-H. Chu // *Acta Mechanica Solida Sinica,* **5**, No.1 (1984), 16.

[11] L. Wang, *Foundations of Stress Waves* (National Defense Industry Press, China, 1985; 2nd Edition, 2005; English Edition, Elsevier, Amsterdam, 2007).

[12] L. Wang // *Int. J. Impact Engineering*, **30**, No.8/9 (2004), 889.

[13] L. Wang and N. Jones // *Acta Mechanica Sinica* **12**, No.4 (1996), 338.

[14] L. Wang // *Explosion and Shock Waves* **2** (1982) 39.

[15] F.P. Bowden and J.E. Field // *Proc. Roy. Soc* **A282** (1964) 331.

[16] J.E. Field // *Phil. Trans. Roy. Soc.* **A260** (1966) 89.

[17] L. Wang, J.E. Field, Q. Sun and J. Liu // *J. Appl. Phys.* **78** (1995) 1643.

[18] I.I. McNaughton, S.W. Chisman and J.D. Booker, In: *Proc 3rd Int Conf on Rain Erosion and Associated Phenomena*, ed. by A.A. Fyall and R.B. King (Royal Aircraft Establishment, Farnborough, UK, 1970).

[19] D.G. Rickerby, *Ph D thesis* (University of Cambridge, 1976).

[20] J.E. Field, D.A. Gorham and D.G. Rickerby, In: *Erosion: Prevention and useful applications,* ed. by W.F. Adler (ASTM, STP 664: ASTM, Philadelphia, PA, 1979), p. 320.

[21] S.B. Menkes and H.J. Opat // *Exp. Mech.* **13** (1973) 480.

[22] T. Nonaka // *J. Appl. Mech*. **34** (1967) 623.

[23] L. Wang, In: *Proc. Int. Symp. on Intense Dynamic Loading and It's Effects*, ed. by Zheng Zhe-Min *et al*. (Science Press, Beijing, 1986) p. 787.

[24] L. Wang, H.-S. Bao, W.-X. Lu // *Journal de Physique*, Colloq. C3, Supplem. **49** (1988) C3, 207.

[25] J. Hopkinson // *Proc. Man. Lit. Phil. Soc.* **40** (1872) 40.

[26] L. Wang and L. Yang, In: *Progress in Impact Dynamics*, ed. by Lili Wang, Tongxi Yu and Yongchi Li (The Press of China University of Science and Technology, Hefei, China,1992), p. 88.

[27] Tang Zhiping, Tian Lanqiao, Chu Chao-Hsiang and Wang Lili, In: *Proc. 2nd Nat. Conf. Explosive Mechanics* (Yangzhou, China, 1981), p. 4-1-12.

[28] Zhou Fenghua, Wang Lili and Hu Shisheng // *Explosion and Shock Waves* **12** (1992) 333.

[29] Liming Yang, Chao-Hsiang Chu and Lili Wang // *Explosion and Shock Waves* **6** (1986) 1.
[30] Liming Yang, Lili Wang and Zhaoxiang Zhu // *Acta Mechanica Sinica* 10 (1994), 176.
[31] A. E. Green and R. S. Rivlin // *Arch. Rat. Mech. Anal*.**1** (1957) 1.
[32] B. D. Coleman and W. Noll // *Arch. Rat. Mech. Anal*.**6** (1960) 355.
[33] B. D. Coleman and W. Noll // *Rev. Mod. Phys.***33** (1961) 239.
[34] Chao-Hsiang Chu, Lili Wang and Daben Xu, In: *Proc. Int. Conf. Nonlinear Mechanics*, ed. by Chien Wei-Zang (Science Press, Beijing, China,1985), p. 92.
[35] A. Kobayashi and Lili Wang, *Quest for Dynamic Deformation and Fracture of Viscoelastic Solids* (Ryoin Publishers, Japan, 2001).
[36] L.M. Yang, V.P.W. Shim and C.T. Lim // *Int. J. Impact Engineering* **24** (2000) 545.
[37] L.M. Yang and V.P.W. Shim // *Int. J. Impact Engineering* **30** (2004) 1099.
[38] Lili Wang, Xixiong Zhu, Shaochu Shi, Su Gan and Hesheng Bao // *Chinese Jour. Aeronautics* **5** (1992) 205.
[39] J. D. Ferry, *Viscoelastic Properties of Polymers* (Wiley, New York, 1980).
[40] F. Schwarzl and A. J. Staverman // *J. Appl. Phys.* **23** (1952) 838.
[41] L.-L. Wang, D.-J. Huang and S. Gan, In: *Constitutive Relation in High/Very High Starin Rates*, ed. by K. Kawata and J. Shioiri (Springer-Verlag, Tokyo, 1996), p. 137.
[42] Lili Wang // *Chinese Jour. of Mechanics, Series A* **19** (2003) 177.
[43] K. Labibes, Lili Wang and D. Pluvinage // *DYMAT Journal* **1** (1994) 135.
[44] D.R. Curran and L. Seaman // *Phys. Reports* **147** (1987) 253.
[45] Danian Chen, S.T.S. Al-Hassani, M.Sarumi and Xiaogang Jin // *Int.l J. Impact Engineering* **19** (1997) 107.
[46] F.L. Addessio and J.N. Johnson // *J. Appl. Phys.* **67** (1990) 3275.
[47] Xiaogang Jin, private communication, 1995.
[48] D.J. Steinberg and R.W. Sharp // *J. Appl. Phys.* **52** (1981) 5072.
[49] S.T.S. Al-Hassanis, Danian Chen and M. Sarumis // *Int. J. Impact Engineering* **19** (1997) 493.
[50] Danian Chen, Yuying Yu and Zhihua Yin // *Int. J. Impact Engineering* **31** (2005) 811.
[51] Danian Chen, Yuying Yu, Zhihua Yin, Huanran Wang, Guoqing Liu and Shugang Xie // *Int. J. Impact Engineering* **31** (2005) 1106.
[52] Fenghua Zhou and Jean-Francois Molinari // *Int. J. Numerical Methods in Engineering* **59** (2004) 1.
[53] Fenghua Zhou and Jean-Francois Molinari // *Int. J. Solids and Structures* **41** (2004) 6573.
[54] Fenghua Zhou and Jean-Francois Molinari // *Computer Methods in Appl. Mech. and Engineering* **194** (2005) 1693.
[55] Fenghua Zhou, Jean-Francois Molinari and Yulong Li // *Engineering Fracture Mechanics* **71** (2004) 1357.
[56] Fenghua Zhou, Jean-Francois Molinari and Tadashi Shioya // *Engineering Fracture Mechanics* **72** (2005) 1383.
[57] Fenghua Zhou, Jean-Francois Molinari and K.T. Ramesh // *Int. J. Solids and Structures* **42** (2005) 5181.
[58] D.E. Grady // *J. Appl. Phys.* **53** (1982) 322.
[59] N.F. Mott // *Proc. Royal Society London* **A189** (1947) 300.
[60] D.E. Grady, In: *Shock waves and high-strain-rate phenomena in metals*, ed. by M.A. Meyers and L.E. Murr (Plenum, London & New York, 1981), p. 181.
[61] L.A. Glenn and A. Chudnovsky // *J. Appl. Phys*. **59** (1986) 1379.
[62] D.S. Dugdale // *J. Mech. Phys. Solids* **8** (1960) 100.
[63] G.I. Barrenblatt // *Advances in Appl. Mech.* **7** (1962) 55.
[64] C. Zener and J.H. Hollomom // *J. Appl. Phys.* **15** (1944) 22.
[65] R.F. Recht // *J. Appl. Phy* **31** (1964) 189.
[66] R.S. Culver, In: *Metallurgical Effect at High Strain Rates*, ed. by R.W. Rohde , B.M. Butcher, J.R. Holland and C.H. Karnes (Plenum Press, NY, 1973), p. 519.
[67] Li-li Wang, In: *Proc. Int. Symp. on Intense Dynamic Loading and It's Effects*, ed. by. Zhe-Min Zheng et al. (Science Press, Beijing, 1986), p. 787.
[68] L.-L. Wang, H.-S. Bao and W.-X. Lu, // *Jour. de Physique*, C3, Supp. **49** (1988) 207.
[69] L.L. Wang, W.X. Lu, S.S. Hu and Z.P. Tang, In: *Macro- and Micro-Mechanics of High-Velocity Deformation and Fracture*, ed. by K. Kawata and J. Shioiri (Springer-Verlag, Belrin, 1987), p. 359.

[70] Wei-Xian Lu, Zai-Qing Lu and Li-Li Wang // *Acta Mitallurgica Sinica* **22** (1986) A317.
[71] Tian-Ping Xu, Li-li Wang and Wei-Xian Lu // *Explosion and Shock Waves* **7** (1987) 1.
[72] Lili Wang, In: *Progress in Impact Dynamics,* ed. by Lili Wang, Tongxi Yu and Yongchi Li (The Press of University of Science and Technology of China, Hefei, 1992), p. 3.
[73] L. Wang and H. Bao, In: *Mechanical Behaviour of Materials-VI*, *Proc. 6th Int. Conf. Mechanical Behavior of Materials, Kyoto, Japan, 29 July-2 August, 1991*, ed. by Joho Masahiro and Inoue Tatsuo (Pergamon Press, 1991), v.1, p. 479.
[74] J.F. Kalthoff and S. Winkler, In: *Impact Loading & Dynamic Behaviour of Materials (1)*, ed. by C. Y. Chem et al. (DGM, 1988), p. 185.
[75] J.F. Kalthoff and S. Winkler // *Appl Mech Rev* **43** (1990) 287.
[76] L. Wang, X. Dong, S. Hu and J. Yu // *Journal de Physique* IV, *Colloque C8, Supp*. **4** (1994) 465.
[77] Xinlong Dong, Jilin Yu, Shisheng Hu, Wu Wang and Lili Wang // *Explosion and Shock Waves* **18** (1998) 62.
[78] Shaochiu Shi, Su Gan and Lili Wang // *Journal of Ningbo University (Natural Science and Engineerring Edition)* **3** (1990) 66.
[79] Hesheng Bao, Weixian Lu, Xinlong Dong and Lili Wang // *Journal of Ningbo University (Natural Science and Engineering Edition)* **4** (1991) 89.
[80] H. Kolsky // *Proc. Phys. Soc.* **B62** (1949) 676.
[81] L.L. Wang, K. Labibes, Z. Azari and G. Pluvinage // *Int. J. Impact Engineering* **15** (1994) 669.
[82] J.E. Field, S.M. Walley, W.G. Proud, H.T. Goldrein and C.R. Siviour // *Int. J. Impact Engineering* **30** (2004) 725.
[83] X. L.Dong, Ming Yan Leung and T. X. Yu // *International Journal of Modern Physics B* **22** (2008) 1062.
[84] Lili Wang, Zhongwei Zhang, Dejin Huang, Xiaohu Yao and Guoyu Chen, In: *Advances in Applied Mechanics*, ed. by Youshi Hong (Science Press, Beijing, 2004), p. 172.
[85] Guo-yu Chen and Li-li Wang, *Protection against Ship-Bridge Collision* (Beijing, China Railway Publishing House, 2006).
[86] Lili Wang, Liming Yang, Dejin Huang, Zhongwei Zhang and Guoyu Chen // *Int. J. Impact Engineering* **35** (2008) 895.